Exploration of BioMat-X

Open Exploration

Open Access Original Article

Fabrication and characterization of pHEMA hydrogel conduit containing GelMA-HaMA IPN for peripheral nerve regeneration

Damla Arslantunali Sahin[1,2], Cagdas Devrim Son[2,3], Vasif Hasirci[1,4,5,6]*

[1]Center of Excellence in Biomaterials and Tissue Engineering (BIOMATEN), Middle East Technical University (METU), Ankara 06800, Türkiye

[2]Graduate Department of Biotechnology, Middle East Technical University (METU), Ankara 06800, Türkiye

[3]Department of Biological Sciences, Middle East Technical University (METU), Ankara 06800, Türkiye

[4]Department of Biomedical Engineering, Acibadem University, Istanbul 34755, Türkiye

[5]Graduate Department of Biomaterials, Acibadem University, Istanbul 34755, Türkiye

[6]Biomaterials Center, Acibadem University, Istanbul 34755, Türkiye

***Correspondence:** Vasif Hasirci, Biomaterials Center, Acibadem University, Istanbul 34755, Türkiye. Vasif.Hasirci@acibadem.edu.tr

Academic Editor: Catherine Le Visage, University of Nantes, France

Received: April 17, 2023 **Accepted:** June 26, 2023 **Published:** February 26, 2024

Cite this article: Sahin DA, Son CD, Hasirci V. Fabrication and characterization of pHEMA hydrogel conduit containing GelMA-HaMA IPN for peripheral nerve regeneration. Explor BioMat-X. 2024;1:34–57. https://doi.org/10.37349/ebmx.2024.00005

Abstract

Aim: Small defects after any injury to the periperal nerves results in self-regeneration. However, for larger defects, suturing or grafting are necessary, which may have limitations. Thus, research on nerve guidence conduits is needed without drawbacks. The aim of the study was to develop hydrogel-based conduits containing interpenetrating network (IPN).

Methods: Methacrylated gelatin (GelMA)-methacrylated hyaluronic acid (HaMA) IPN was filled the poly(2-hydroxyethylmethacrylate) (pHEMA) the outer conduit. Schwann cells (SCs) were used on the pHEMA and the distal end of the tube was injected with netrin-1 to support model SH-SY5Y cells.

Results: ^{1}H-nuclear magnetic resonance (^{1}H-NMR) showed that methacrylation degrees were 94% ± 2% for GelMA and 60% ± 7% for HaMA. The fraction of HaMA increased the degradation rate; pure HaMA degraded in 3 weeks, while pure GelMA in more than 5 weeks. An increase in the fraction of 2-hydroxyethylmethacrylate (HEMA) from 20% to 56% decreased the porosity and the pore size, significantly. SH-SY5Y cells migrated along the conduit in the presence of netrin-1. NeuN expression was increased in 2 weeks indicating neuronal activity.

Conclusions: SH-SY5Y cells produced neurites in the IPN. pHEMA conduit including GelMA-HaMA IPN is a good candidate for peripheral nerve regeneration applications. As future studies, the conduit will be tested *in vivo* for nerve regeneration.

Keywords

Peripheral nerve injury, axon regeneration, nerve guidance conduit, hydrogel, poly(2-hydroxyethylmethacrylate), methacrylated gelatin, hyaluronic acid, interpenetrating network

Introduction

Because of physiological impairments, injury to the peripheral nerves has a significant impact on a patient's quality of life. The increase in the number of injuries indicates that PNI is a worldwide clinical problem; PNI was diagnosed in 551,612 patients during 2009–2018, of whom nearly 22% had a history of physical activity and sports [1]. The axons have the ability to regenerate when the defect is small (≤ 3 mm) and follow 3 main cascades to do so: Wallerian degeneration, axonal regeneration, and end-organ reinnervation [2]. The severity and the type of the injury determine the success of the self-regeneration or end to end surgery. When the injury causes complete transection and the gap between the proximal and distal parts is ≥ 3 mm, microsurgical interventions become compulsory grafting or use of artificial nerve guides is applied [3]. End-to-end suturing is not possible when the gap is larger because the tension created during suturing becomes excessive (≥ 3 mm). Methods used for larger defects (≥ 10 mm) like autografting, xenografting or allografting may also have some disadvantages such as donor site morbidity, immune reaction, cross contamination and limited supply of donor tissue. Thus, considering the limitations of the end-to-end suturing and grafting methods, the nerve conduits have emerged among researchers [4, 5].

The gold standard strategy (autografting) includes the fibrin cable production by the patient for nerve regeneration in the nerve conduits. When a hollow nerve conduit is used in the treatment of a peripheral nerve damage, its lumen is filled with a fluid that infiltrates among the undamaged fibrin cables (a "blood clot") that extend over the gap between the proximal and distal nerve stumps. Fibrin cables operate as a microarchitectural cue to direct migrating Schwann cells (SCs) into the damage site [6]. Extracellular matrix (ECM) proteins like collagen and laminin are secreted by the cells (neuronal or non-neuronal) which migrate to the injury site. Scar formation is decreased by this highly controlled environment and nerve stumps that produce growth factors [7]. Nerve conduits aim to mimic the autografts in terms of supporting axon growth. General properties for the scaffold constructs should include to be suitable for cell migration, proliferation and differentiation. Nerve conduits have been designed using a variety of biopolymers. Due to their poor mechanical properties, the polymers are difficult to be fabricated. On the other hand, the slow biodegradability of the synthetic polymers limits their use in the development of nerve conduits. Hybrid conduits composed of both synthetic and natural biopolymers are an obvious choice for use in nerve conduits. Natural polymers such as hyaluronic acid (HA) [8], collagen [9], gelatin [10], chitosan [11], alginate [12]; synthetic polymers such as polydimethylsiloxane [13], polylactic acid [14], polyglycolic acid [15] and poly(2-hydroxyethylmethacrylate) (pHEMA) [16] and also their blends [17, 18] have been used for nerve tissue engineering applications. Nervous tissue is one of the soft tissues and its ultimate tensile strength (UTS) is 1,400 kPa and tensile modulus is 576 kPa [19]. Thus, one of the most appropriate materials to be used in nerve tissue engineering applications are hydrogels due to their mechanical properties and the hydrated structure. Hydrogels have ability to absorb water and become soft rubbery; making them suturable and having mechanical properties similar to nerve tissue [20]. In the present study, pHEMA hydrogel nerve conduit is presented together with methacrylated gelatin (GelMA)-methacrylated HA (HaMA; GelMA-HaMA) interpenetrating network (IPN) filler. To support and guide axonal regeneration, SCs were seeded into the nerve conduits, and the distal part of the conduit was loaded with netrin-1 protein. pHEMA hydrogel is hydrophilic, transparent, biocompatible, and non-degradable, and has mechanical properties to be customised according to the application such as wound dressings, soft contact lenses, ocular drug delivery, artificial skin, artificial cornea, catheters, breast augmentation, and nerve tissue engineering [21]. The GelMA-HaMA filler of the presented nerve conduit was considered to be supportive for regenerating axons because of its degradable sturucture. The degradation profile of the IPN structure can be adjusted by changing concentrations of the mixture and initiators, which makes the structure attractive for tissue engineering applications [22].

SCs are support cells that aid in axonal regeneration following injury in the peripheral nervous system (PNS) by secreting neurotrophins. In Wallerian degeneration, neuronal and non-neuronal cells release cytokines that stimulate SCs to produce neurotrophins like brain-derived neurotrophic factor (BDNF) and nerve growth factor (NGF) [23]. SCs' migration, longitudinal organization, and fibrin cable creation all occur on their own for nerve gaps smaller than 3 mm. Thus, SCs are support cells that aid axonal regeneration

following injury in the PNS by secreting neurotrophins. On the otherhand for longer nerve gaps, nerve regeneration typically requires SCs to be introduced to the injury site [24–27]. The production of nerve guidance conduits frequently uses supporting factors for axonal regeneration in addition to support cells. It has been demonstrated that netrin proteins are useful for guiding circumferential axonal projections [28]. Initially, netrin-1 was recognized as a traditional axonal guidance molecule with potent axon elongation abilities. Thus, to support axonal regeneration and guidance in the current work, SCs and netrin-1 were added. SH-SY5Y are well characterized cells and for this reason they have been in use since 1980s in tissue engineering and neurobiological applications. These cells were originally obtained from bone marrow biopsy of a blastoma and possess biochemical and functional properties which are suitable for studying neuronal extensions and organizations [29]. Therefore, SH-SY5Y cells were used as model cells in this study.

This study was aimed to design novel composite nerve guide and test it under *in situ* and *in vitro* conditions. The nerve guide composed of pHEMA was prepared and the cylindrical structure was filled with GelMA-HaMA IPN. The nerve guide was evaluated in terms of survival, production of neurite outgrowth and migration of the model SH-SY5Y cells. The positive effects of SCs and netrin-1 protein were shown on the neural cells *in vitro* and the final suturable nerve guide was developed to be used in further peripheral nerve regeneration applications.

Materials and methods

Materials

Gelatin (type A from porcine skin), HA sodium salt from *Streptococcus* equi (< 1% protein), methacrylic anhydride (94%), 1-[4-(2-hydroxyethoxy)-phenyl]-2-hydroxy-2-methyl-1-propan-1-one (Irgacure 2959), dimethylformamide (DMF), 2-hydroxyethyl methacrylate (> 99%), ethyleneglycol dimethacrylate (98%), *N*,*N*-thiazolyl blue tetrazolium bromide, sodium cacodylate, glutaraldehyde (25%), bovine serum albumin (BSA), mouse anti-human collagen type I, Alexa Fluor 532-conjugated anti-mouse immunoglobulin (Ig) antibody, 4',6-diamidino-2-phenylindole dihydrochloride (DAPI) and FITC-conjugated phalloidin were purchased from Sigma-Aldrich (United States). Triton-X and dimethyl sulfoxide (DMSO) 100 were obtained from AppliChem (Germany). Dulbecco's Modified Eagles Medium (DMEM) with high glucose, fetal bovine serum (FBS) is purchased from Gibco (Thermo Fisher Scientific, United States). Penicillin/streptomycin (Pen/Strep; 100 units/mL, 100 µg/mL) was purchased from Fluka (Switzerland). Anti-neuron specific β-tubulin class III (β-III tubulin) antibody, anti-NeuN, Donkey anti-Rabbit IgG H&L (DyLight®488) secondary antibody were purchased from Abcam (United States). SH-SY5Y (neuroblastoma cell line, human derived, ATCC CRL-2266.Adh) and SCs (SW 10, ATCC CRL-2766) were purchased from ATCC (United States).

Preparation of pHEMA nerve guides

The molds containing an outer glass tube together with an innner cylinder and lids printed from Dental SG Resin by stereolithography (SLA 2, Formlabs, United States), were used to prepare cylindrical pHEMA guides (Figure 1A). Solution polymerization was used to prepare pHEMA as described earlier [30]. Briefly, distilled water and 2-hydroxyethylmethacrylate (HEMA) monomer were mixed (44%, 50%, 55%, 58%, v/v; total volume: 3 mL) and crosslinker [ethylene glycol dimethacrylate (EGDMA)] was added (0.4%, v/v; in monomer). Then, Irgacure 2959 was added to the reaction mixture (0.025%, w/v) as an initiator. In order to remove oxygen the solution was purged with nitrogen and reaction was performed under ultraviolet light (UV; 365 nm) for 10 s. The pHEMA was incubated in excess distilled water to remove unreacted molecules were then lyophilized for 6 h. pHEMA hydrogels were then impregnated with collagen by immersing in a collagen solution (1% in acetic acid, w/v) for overnight. The hydrogels were lyophilized after washed with distilled water. Lyophilized pHEMA conduits had outer diameter of 1.2 cm, inner diameter of 0.2 cm and the height of 1.3 cm.

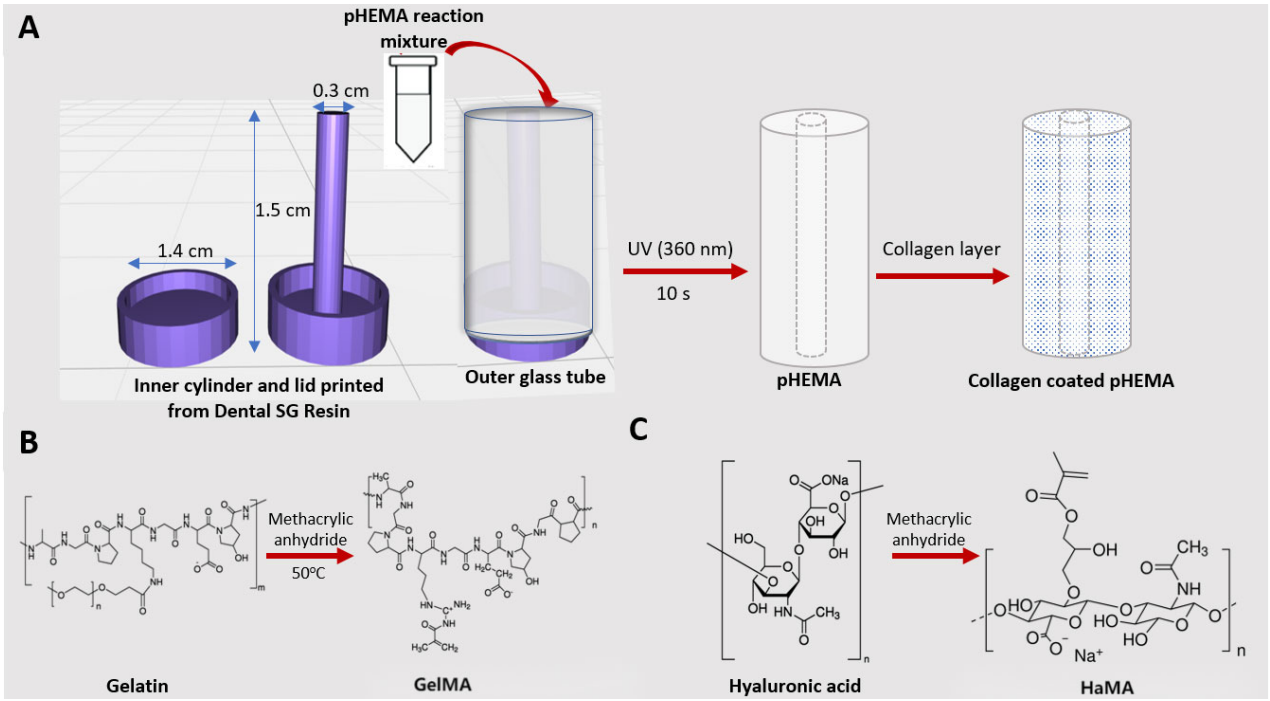

Figure 1. Preparation of conduit materials. A) pHEMA mold sketch of the SLA system; B) methacrylation of gelatin; C) methacrylation of HA

Synthesis of GelMA and HaMA

According to Shirahama et al. [31] and Smeds [32], GelMA and HaMA were synthesized. Briefly, methacrylic anhydride (0.1 mL/g gelatin) was added to the solution after type A Porcine Skin gelatin was dissolved in carbonate buffer (CB; 20%, w/v; total volume: 200 mL; 0.25 mol/L CB pH 9) (Figure 1B). The mixture was then incubated at 50°C for 3 h. Dimethyl formamide was added dropwise into the solution after the HA solution [2:3, DMF:distilled water (dH_2O)] was dissolved in dH_2O (1%, w/v; total volume: 200 mL) and kept at room temperature (RT) for 24 h. The solution was incubated at 40°C for 1 h. Methacrylic anhydride (5%, v/v) was added to the solution, the pH was set to 8–9, and the mixture was monitored for 5 h (Figure 1C). To eliminate extra methacrylic acid (MA) and salts, the solutions were filtered and dialyzed in a dialysis tube (CO 10,000 da) against distilled water for three days at 37°C. The solutions were dialyzed and then lyophilized for a week. The resulting GelMA and HaMA were kept in storage at 4°C.

Determination of MA content of GelMA and HaMA with nuclear magnetic resonance

Gelatin, GelMA (5 mg/mL), HA, and HaMA were dissolved in deuterium oxide (D_2O, 5 mg/mL) at 60°C to calculate the methacrylation degrees. Nuclear magnetic resonance (NMR) spectra were collected using a Bruker DPX 400 spectrometer at a ^1H resonance frequency of 400 MHz.

Preparation of GelMA-HaMA IPN

The IPN matrix for the GelMA-HaMA was produced by dissolving GelMA and HaMA in phosphate buffered saline (PBS, 1% HaMA, w/v) in various ratios (a-5:95, b-10:90, c-15:85, and d-20:80; total volume of stock solution: 5 mL). Irgacure 2959, a photoinitiator, was incorporated (1%, w/v), and polymerized for 5 s at a distance of 3 cm under UV (200 µL of stock solution in 96 well plate, 365 nm, 15 W/cm^2, OmniCure S2000 UV Lamp).

FTIR analysis

The surface chemistries of gelatin, uncrosslinked and crosslinked GelMA and HA, crosslinked and uncrosslinked HaMA were studied by FTIR-ATR spectroscopy (Perkin Elmer Spectrum, Frontier, Massachusetts, United States) to assess the extent of methacrylation and crosslinking in the range 400–4,000 cm^{-1}. Four scans were performed.

Degradation of GelMA-HaMA IPN

The degradation behavior of GelMA-HaMA IPNs (1 cm in diameter and about 0.5 cm in height) was investigated by weighing and incubating IPNs in PBS (10 mmol/L, pH 7.4) and cell culture media for 4 weeks at 37°C. After getting samples, lyophilizing them, and then rinsing them in distilled water, weight loss was measured every day. Degradation was calculated as a percent weight loss using Equation 1.

$$\text{Remaining weight (\%)} = \frac{w_0 - w_d}{w_d} \times 100 \quad (1)$$

where w_0 is the initial dry weight and w_d is dry weight after incubation.

Water content determination and swelling of pHEMA hydrogels

Weighed and then placed in PBS for 24 h, pHEMA hydrogels (1 cm in diameter and about 0.5 cm in height) and GelMA-HaMA matrix's ability to swell was assessed. They were measured for weight after swelling for 24 h. The water content was calculated using Equations 2 and 3.

$$\text{WC (\%)} = \frac{w_s - w_d}{w_s} \times 100 \quad (2)$$

$$\text{Swelling (\%)} = \frac{w_s - w_d}{w_d} \times 100 \quad (3)$$

where WC (%): is water content (%, w/w), w_s wet weight and w_d dry weight of the samples.

Water contact angle determination of pHEMA hydrogels

Water contact angle of pHEMA hydrogels were measured at their swollen state after incubating pHEMA hydrogels in distilled water for 24 h at RT. An optical tensiometer (One Attension, Biolin Scientific, Finland) was used to measure the contact angles after the excess water had been removed. Three different locations on the surfaces provided three different results.

Mechanical test of pHEMA hydrogels

Mechanical properties of pHEMA hydrogels were determined at their swollen state after incubating pHEMA hydrogels in distilled water for 24 h at RT. CellScale, Univert (Canada), was used to measure the tensile modulus of the polymers using pHEMA hydrogels with dimensions of 30 mm length and 10 mm width. The samples were clamped (gauge length: 10 mm), and straining was done at a rate of 20 mm/min. Following the results, the equations below were used to determine the elastic modulus (E, N/mm^2), strain at break ε_f, and UTS:

$$\text{UTS} = \frac{\text{F}}{\text{A}} \quad (4)$$

$$\text{E} = \frac{\Delta\text{F}}{\text{A}} \times \frac{\text{L}}{\Delta\text{L}} \quad (5)$$

$$\varepsilon_f\ (\%) = \frac{\text{L}_\text{f} - \text{L}_\text{i}}{\text{L}_\text{i}} \times 100 \quad (6)$$

where F is applied force (N), A is area (mm^2), L is length (mm), L_i is initial length (mm) and L_f is final length (mm).

Scanning electron microscope and porosity analysis of pHEMA hydrogels

After lyophilization of the polymer samples (Labconco, FreeZone6p Plus, United States) for 8 h, they were attached on scanning electron microscope (SEM) stubs with carbon tapes. The specimens were coated with a thin layer of gold using sputter coating before being studied under a SEM (Quanta FEI, United States).

ImageJ (NIH, United States) was used to examine pore sizes and porosities of the polymers. Three different hydrogels were used to calculate the porosities and pore sizes. The porosities were calculated by dividing total pore area with the surface area. The SEM micrographs were converted into black and white image by using "threshold" method of ImageJ and then the ratio of black regions (pores) to the total area was calculated to obtain the porosity of the surfaces. For pore size determination, the diameters of minimum 30 pores from each SEM micrograph were measured and the mean values were calculated in micrometers.

In vitro studies

SC seeding on pHEMA hydrogels

Mouse neuronal SCs (ATCC CRL-2766) were seeded on cylindrical pHEMA hydrogels. The cells were maintained in a DMEM high glucose growth medium that contains FBS (10%, v/v), and penicillin/streptomycin (100 units/mL, 100 g/mL, respectively). Before cell seeding, pHEMA membranes were sterilized for 30 min. by UV (280 nm). In order to promote adhesion, after 10^5 cells/scaffold were seeded and they maintained for 2 h in a humidified 5% CO_2 incubator.

SH-SY5Y neuroblastoma cell seeding in GelMA-HaMA IPNs

The GelMA-HaMA gels were developed into films to analyze cell proliferation on them. The films were sterilized for 30 minutes on each side using UV (280 nm) light. Cells (10^5) were seeded on each GelMA-HaMA film after the cells had been cultured in DMEM high glucose tissue culture medium FBS (10%, v/v) and penicillin/streptomycin (100 units/mL:100 g/mL, respectively) and counted. A humidified 5% CO_2 incubator was used to incubate the films. Full medium was added after 2 h, and it was replaced every 2 days. SH-SY5Y cells were added to the GelMA-HaMA reaction mixture and crosslinked under UV (365 nm, 15 W/cm^2, OmniCure S2000 UV Lamb) for 5 s (distance: 3 cm) to produce the final conduit.

Cell attachment and proliferation

MTT assay

For 4 weeks of cell culture, 3-(4,5-dimethylthiazol-2-yl)-2,5-diphenyltetrazolium bromide (MTT) cell proliferation assays were performed on both the pHEMA hydrogels and the GelMA-HaMA IPNs. As with the previous procedures in the literature, cell number was determined by reducing MTT to a purple formazan by live cells [33].

Live-dead cell viability assay

The live dead cell viability assay was used to assess the viability of Schwann and SH-SY5Y cells on days 1, 7, and 14 following seeding on pHEMA hydrogels and GelMA-HaMA films, respectively. The German Zeiss LSM 9100 microscope was used to view the green live cells (calcein-stained) and red dead cells (ethidium-bromide-stained) and then to count the cells, ImageJ was used.

Confocal laser scanning microscopy examination of the cells

Cytoskeleton and nucleus staining

On days 1, 7, 14, and 21, the cells were fixed for 15 min with 4% (w/v) paraformaldehyde at RT before being permeabilized for 5 min with 1% (v/v) triton X-100 in PBS (pH 7.4). Samples were incubated in BSA (1%, w/v in PBS) for 30 min at 37°C to prevent non-specific binds. The samples were first stained for the cytoskeleton with Alexafluor 488-Phalloidin (1:200, w/v in 0.1% BSA) for 1 h at RT, and then the nuclei were stained with DAPI for 30 min at RT.

β-III Tubulin and NeuN antibody staining

According to the manufacturer's instructions, SH-SY5Y cells were stained with NeuN antibody and β-III tubulin. The cells were briefly treated in blocking solution (1% BSA, 0.1% Tween, 20.0% goat serum, and 0.3 mol/L glycine in PBS) after being fixed. NeuN antibodies (1:200 in 0.1% BSA-PBS) and anti-β-III tubulin antibodies (1:100 in 0.1% BSA-PBS, respectively) were added and incubated overnight at 4°C. For

secondary antibody staining, cells were incubated at 37°C for 1 h with both Alexa Fluor 488 labeled anti-mouse antibody made in goat and Alexa Fluor 647 labeled antirabbit antibody made in donkey, both diluted in 0.1% BSA (1:100). Cells were then washed and analyzed with confocal laser scanning microscopy (CLSM).

Construction of the final conduit and netrin-1 loading

IPNs were crosslinked following SH-SY5Y cells were introduced to the GelMA-HaMA reaction mixture, and they were subsequently incubated for 7 days. On pHEMA hydrogels, SCs were seeded and cultured for 7 days. In cylindrical pHEMA hydrogels, SH-SY5Y containing IPNs were inserted, and the remaining volume in the tube was filled with cell-free IPN (Figure 2). After 7 days of incubation, netrin-1 protein (100 g/mL, final amount in each construct: 200 ng) was injected into one side of the finished construct. After incubating the cells for 7 days, CLSM analysis was performed on them.

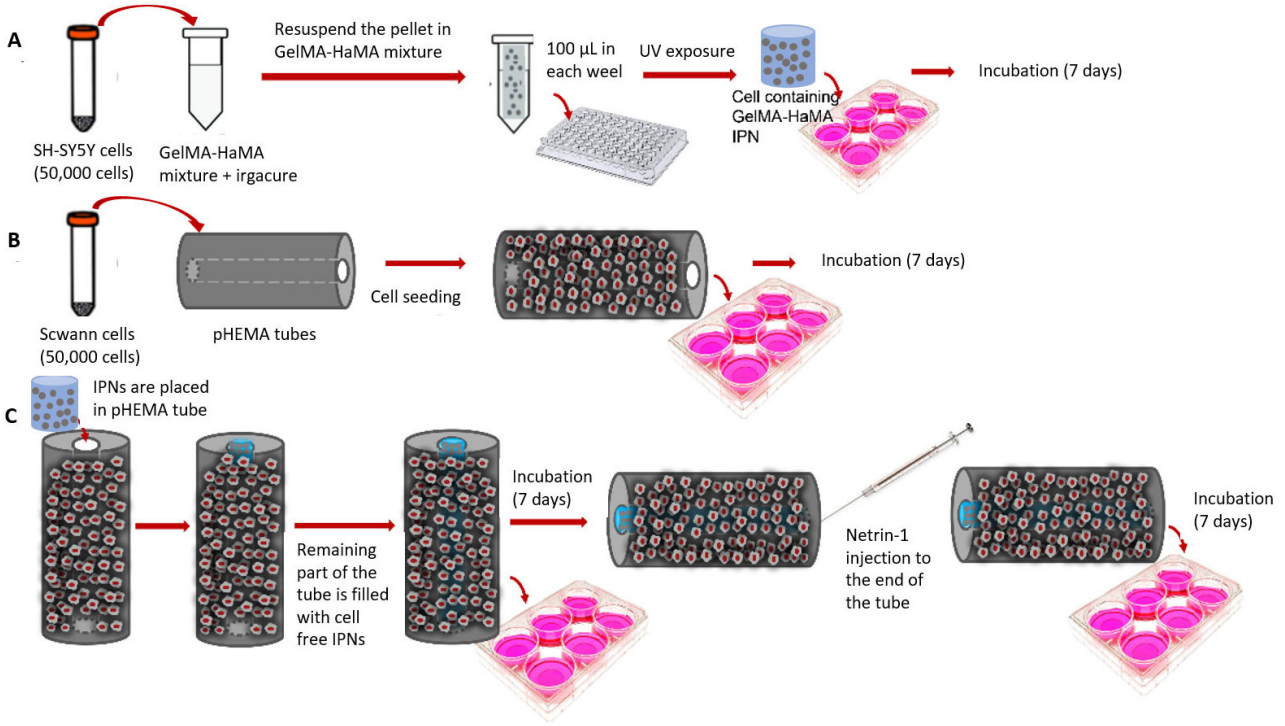

Figure 2. Construction of the final structure. A) Formation of GelMA-HaMA IPN loaded with SH-SY5Y cells; B) SC seeding on pHEMA conduit exterior; C) complete conduit formedon by addition of SH-SY5Y loaded IPNs into the central cavity of pHEMA conduits

Statistical analysis

The characterization and *in vitro* tests were carried out in triplicate. By using the 1-tail Student's *t*-test and analysis of variance (ANOVA), arithmetic means and standard deviations were used to identify significant differences between the mean values in the control and test groups. The differences were regarded as statistically significant with the $P \leq 0.05$.

Results

MA content of GelMA and HaMA with NMR

Methacrylation extent of GelMA and HaMA were determined with ^{1}H-nuclear magnetic resonance (^{1}H-NMR). The degree of methacrylation (DM) was calculated by using Equation 7 [34, 35]. ^{1}H-NMR spectra of gelatin and GelMA was shown in Figure 3A, the results were normalized to the phenylalanine signal. The signal increase in the protons of methacrylate vinyl group of MA (5.4–5.7 ppm, red arrow on Figure 3A) and the signal decrease of the protons of methylene of lysine signal (2.9 ppm) shows the methacrylation and DM was found as 94% ± 2%.

$$DM = 1 - \frac{\text{Lysine methylene proton of GelMA}}{\text{Lysine methylene proton of Gelatin}} \times 100 \quad (7)$$

HA and HaMA ^{1}H-NMR spectra are shown in Figure 3B. Since the anomeric proton signals at 2.07 ppm are proportional to the HA concentration and are unaffected by the methacrylation process, the ^{1}H-NMR spectra were normalized accordingly. DM was calculated by the ratio of the relative peak integrations of the methacrylate protons (6.1, 5.6, and 1.85 ppm) and methyl protons of HA (1.85 ppm) represented by arrows on Figure 3B [36]. The DM was calculated as 60% ± 7% for the synthesized HaMA.

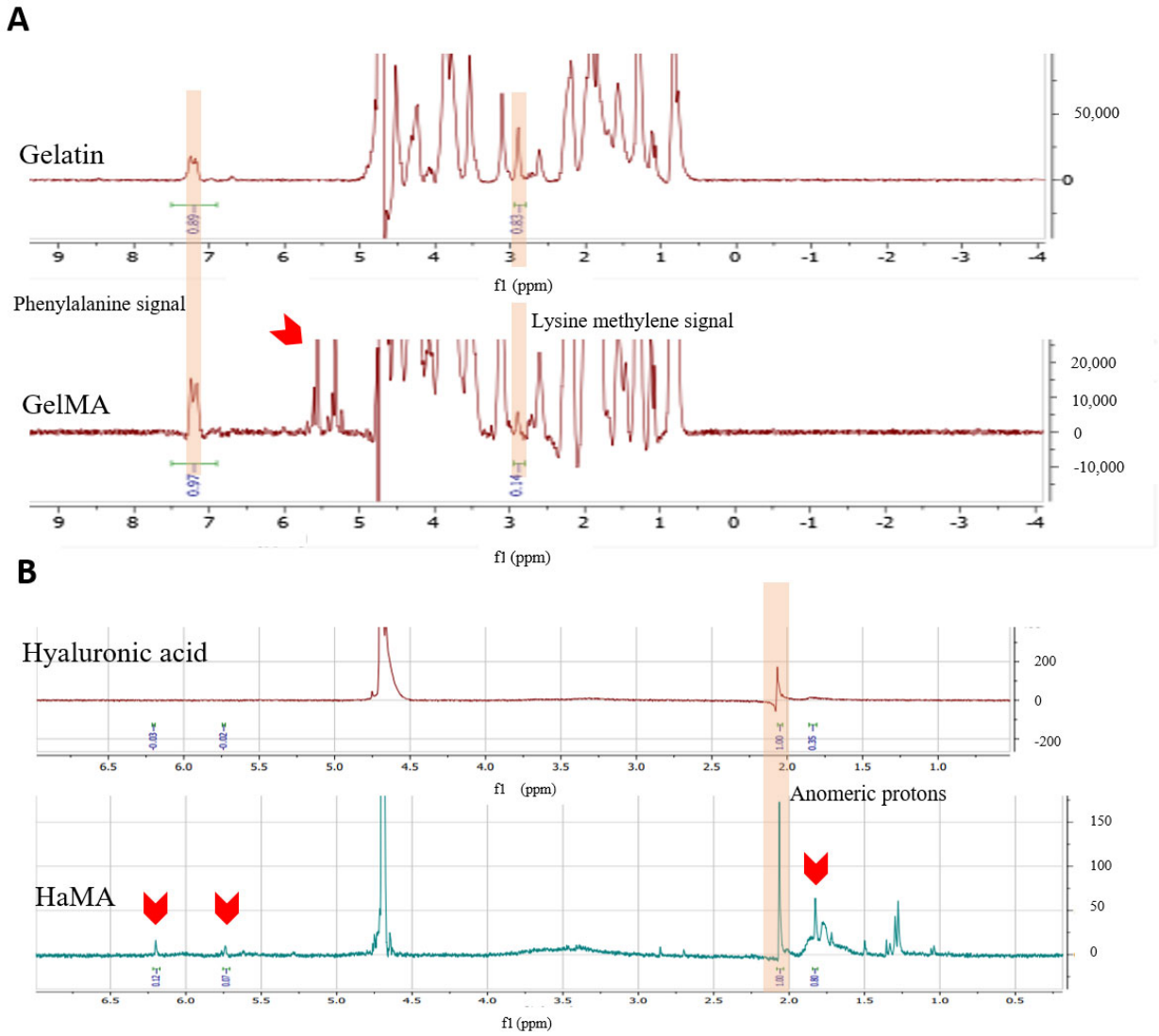

Figure 3. ^{1}H-NMR and FTIR analyses of GelMa and HaMA. A) ^{1}H-NMR spectra of gelatin and uncrosslinked GelMA (normalized to the signal at 7.3 ppm); B) ^{1}H-NMR spectra of HA and uncrosslinked HaMA (normalized to the signal at 2.07 ppm). Red arows show methacrylation bonds

FTIR of GelMA-HaMA IPNs

The usual FTIR spectrum of gelatin and GelMA is presented in Figure 4A, which exhibits vibrations at 3,300 cm^{-1} (O-H stretching vibrations), 2,922 cm^{-1} (C-H stretching), 1,640 cm^{-1} (C-O stretching, Amide I), and 1,525 cm^{-1} (N-H bending, Amide II). Their intensities increased after the methacrylation of the gelatin, and they decreased back after the crosslinking of GelMA because the crosslinking reaction utilized all the hydroxyl group (-OH) groups around 3,300 cm^{-1} [37, 38].

The FTIR spectra of HA, HaMA and crosslinked HaMA are shown in Figure 4B. A new peak at 1,731 cm^{-1} was observed in HaMA when compared to the HA related with the methacrylation and C=C bond peak

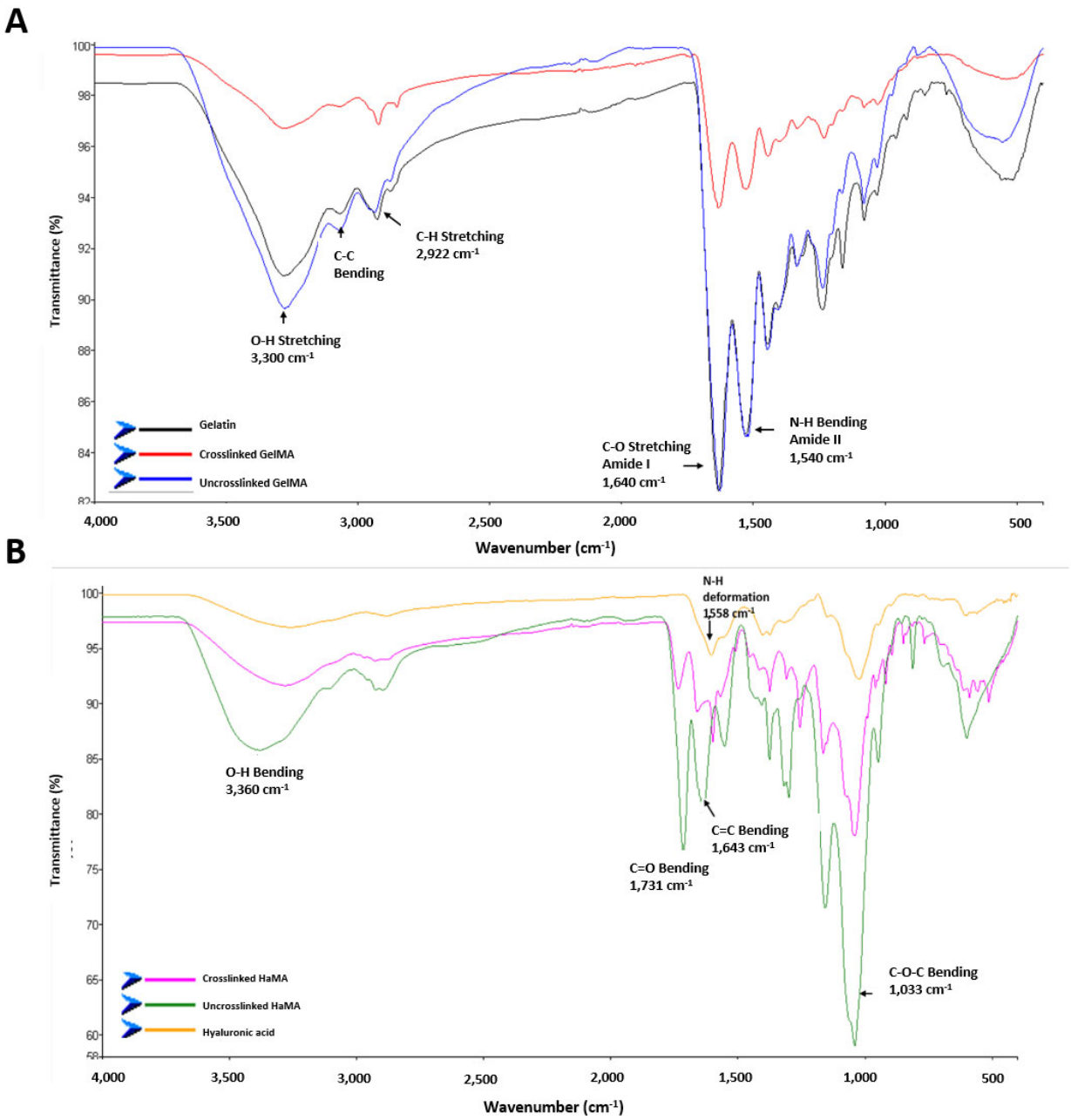

Figure 4. FTIR analyses of GelMa and HaMA. A) FTIR spectra of gelatin, uncrosslinked GelMA and crosslinked GelMA; B) FTIR spectra of HA, uncrosslinked and crosslinked HaMA

was also increased at 1,643 cm^{-1} [39]. Then upon crosslinking reaction the peaks decreased showing that methacrylate groups went into reaction. A N-H deformation signal was observed at 1,558 cm^{-1} because the nitrogen atom of HA did not react with MA. The -OH group's intra- and intermolecular stretching vibration is linked to the peak at 3,360 cm^{-1} [40]. The units of the C-O-C hemiacetalic system are related to the peak at 1,033 cm^{-1}.

Water content, swelling and degradation of GelMa-HaMA IPNs

Hydrogels absorb water and swell in aqueous media, reducing their mechanical properties (e.g., stiffness) which are important in their application [41]. Pure GelMA and HaMA hydrogels had water contents of 86% and 88%, respectively, and these values were nearly identical (Figure 5A). To understand how mixing in different ratios affect water content, IPNs were prepared in different combinations that resulted in very similar water contents (87%, 88%, 84%, 92% for the ratios of 5:95, 10:90, 15:85, 20:80, respectively). Thus, all the water content values were above 80% for all of them.

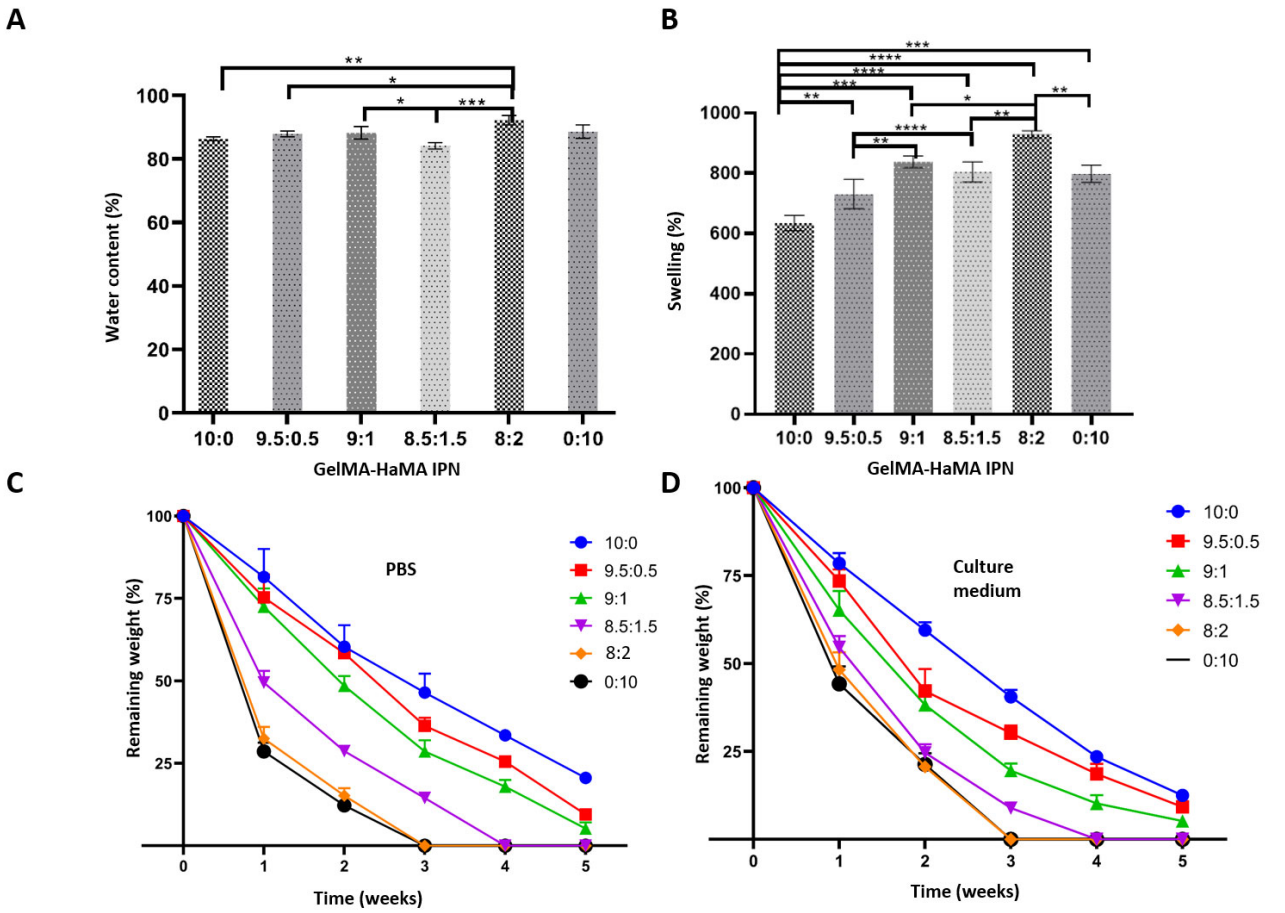

Figure 5. Characterization of the GelMA-HaMA IPNs prepared at different ratios. A) Water content; B) swelling; C) degradation profile of IPNs in PBS; D) degradation profile of IPNs in cell culture medium. Statistical differences (* $P \leq 0.05$, ** $P \leq 0.01$, *** $P \leq 0.001$, **** $P \leq 0.0001$) are indicated

To demonstrate the impact of adding HaMA to the IPNs, the swelling degree of the IPNs was computed (Figure 5B). The findings demonstrated that IPN's swelling capabilities were enhanced by an increase in HaMA content.

The biodegradability of the hydrogels of GelMA, HaMA and GelMA-HaMA IPNs was studied in PBS (Figure 5C) and culture medium (Figure 5D) for 5 weeks and weight loss during this period was determined gravimetrically. During this period GelMA lost 75% of its weight, while HaMA completely degraded in 3 weeks. Hydrogels with IPN structure were more stable when compared to the pure HaMA. Increasing the fraction of HaMA in IPN structure increased the weight loss rate (Figure 4C and D). A statistically significant difference in the degradation profile was not observed in PBS and medium.

Porosity, water content and swelling of pHEMA hydrogels

The outer cylindrical structure of the final conduit prepared in the present study was composed of pHEMA. SEM micrographs of the hydrogels with different water contents are presented in Figure 5. Closed pores were observed on the surfaces of the hydrogel produced with 44% water in the reaction mixture (Figure 6). As the water content of the hydrogels was increased during synthesis, more porous structures developed. The images were analyzed with NIH ImageJ to determine porosity and pore sizes (Figure 7A and B, Table 1). Hydrogels with water concentrations of 44%, 50%, 55%, and 58%, respectively, were found to have porosities of 17%, 33%, 52%, and 50%. Additionally, it was found that the average pore diameters for the hydrogels with water concentrations of 44%, 50%, 55%, and 58%, respectively, are 40.75 µm ± 8.59 µm, 55.09 µm ± 7.15 µm, 15.24 µm ± 3.05 µm and 15.44 µm ± 2.05 µm. The micrographs show the pores of the hydrogels in the dry state; thus, the pores are not the actual pores when the hydrogel is in a swollen state on which the cells are seeded. The hydrogels with the highest capacity of swelling have the smallest pore sizes in their dry states, because they shrink more than the hydrogels with less capacity for swelling.

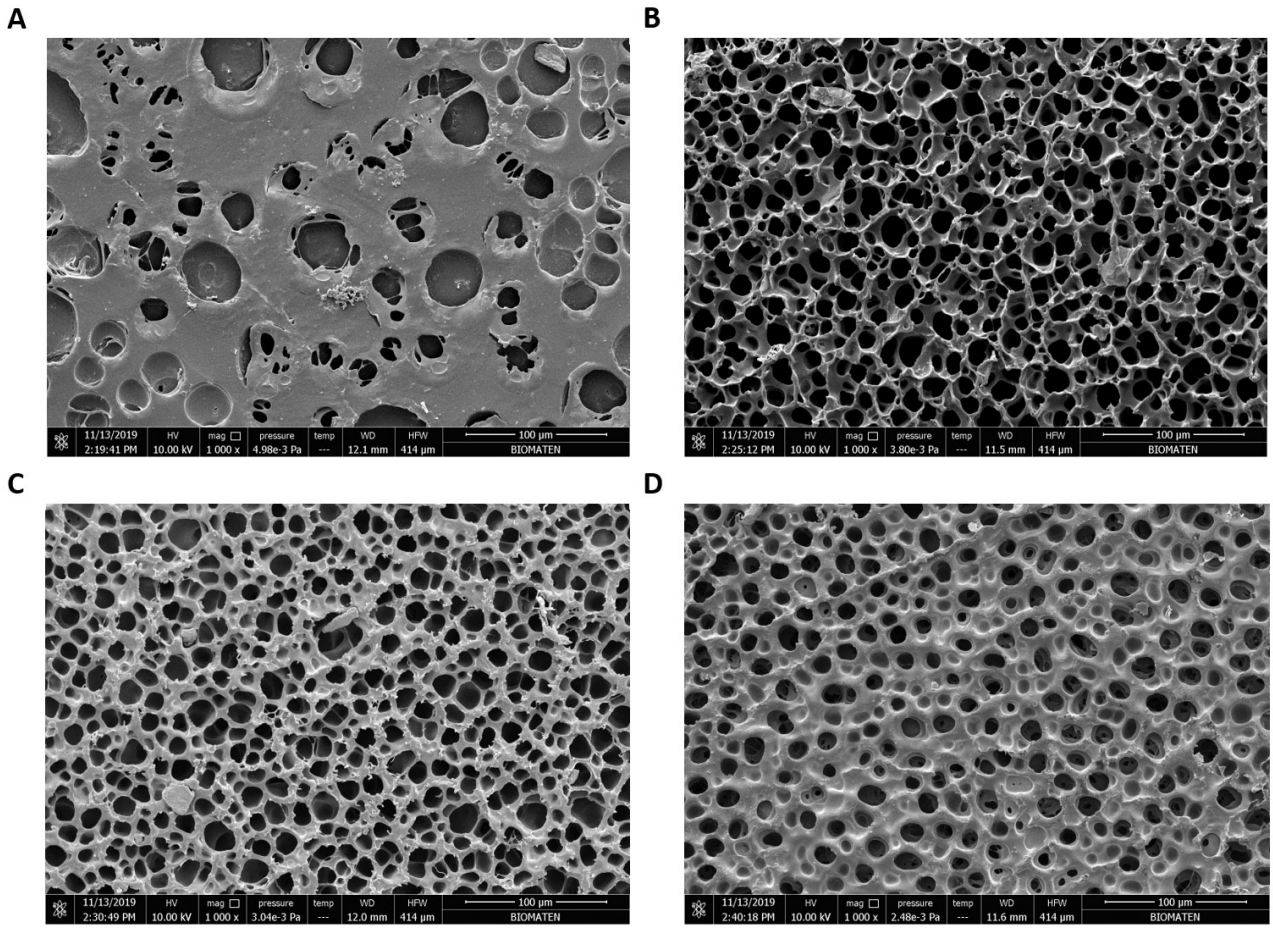

Figure 6. SEM micrographs of pHEMA hydrogel surfaces prepared with different water contents. A) 44%; B) 50%; C) 55%; D) 58%. Scale bar: 100 µm

Table 1. Porosity, pore size and water content (%) of pHEMA hydrogels prepared with different water contents

Water content of the reaction mixture (%)	Porosity (%)	Pore sizes (µm)	Water content after swelling (%)
44	17	40.75 ± 8.59	40.27 ± 1.20
50	33	55.09 ± 7.15	42.80 ± 1.24
55	52	15.24 ± 3.05	47.60 ± 1.34
80	50	15.44 ± 2.05	52.17 ± 0.50

By determining the ratio of water absorption, the equilibrium water contents of pHEMA hydrogels produced with various water compositions were calculated (Figure 7C, Table 1). The water content of the hydrogels became from 40% to 52% as the amount of water in the reaction mixture increased. The difference between the hydrogels of different water contents in the preparation mixture was found statistically significant. To further understand the ability of hydrogels to preserve their integrity, the swelling profiles of pHEMA tubes with various concentrations of water were determined. The gels swelled to their equilibrium value when the tubes were submerged in water (days 2, 4, 6, and 8), and they lost the same quantity of water when they dried (Figure 7D). The gels prepared in this study maintain their ability to reswell repeatedly, without any sign of hysteresis making.

Water contact angle of pHEMA hydrogels

Contact angle is an important factor which is used for understanding wettability of a solid surfaces. It is determined by the balance between adhesive and cohesive forces [18]. The contact angles of membranes were found as 50.8° ± 15.4°, 31.0° ± 7.6°, 17.8° ± 10.2° and 6.2° ± 4.5° for pHEMA hydrogels having different water content in reaction mixture (Table 2). As a result, the hydrophobicities of pHEMA tubes are decreasing with increasing water content in the preparation mixture.

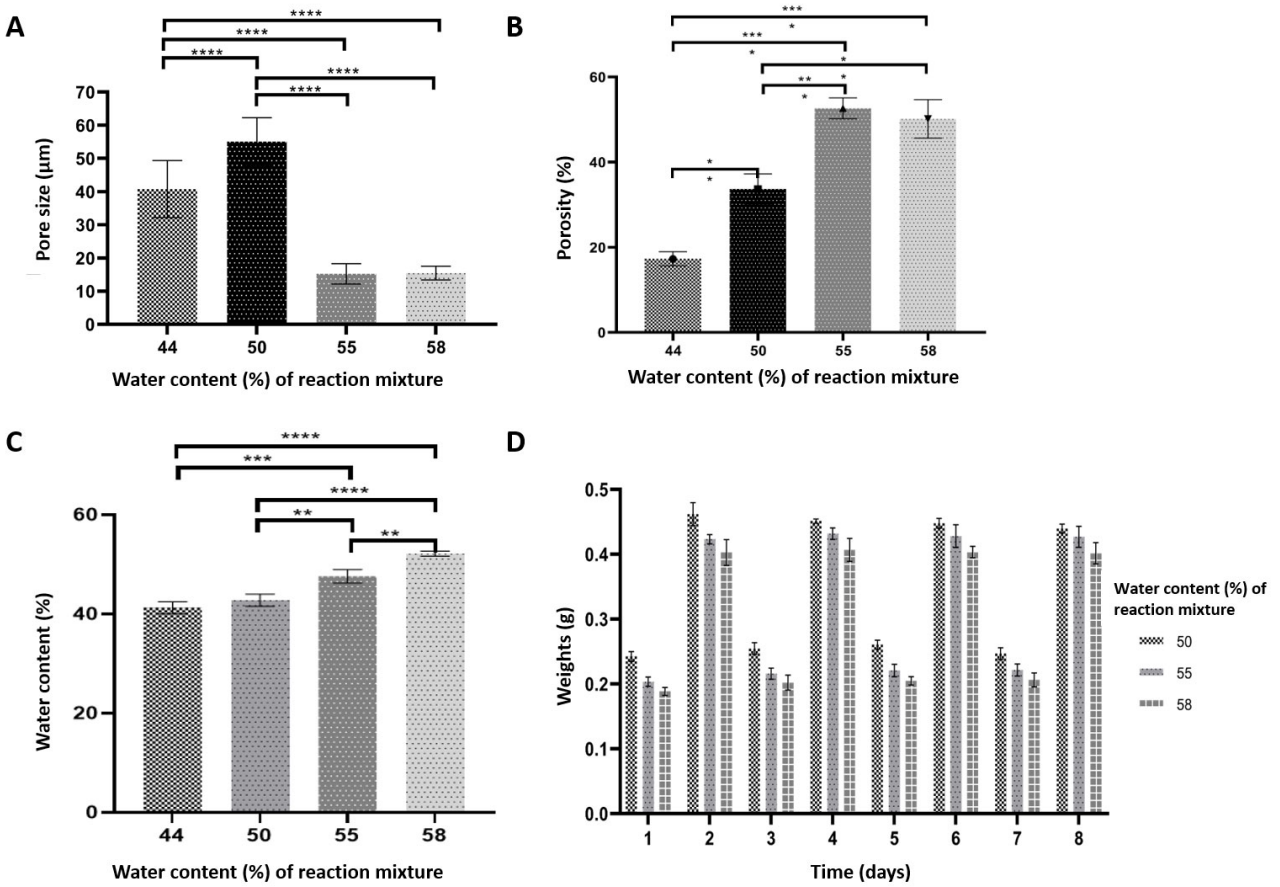

Figure 7. Characterization of pHEMA hydrogels prepared with different water content in reaction mixture (44%, 50%, 55%, 58%; v/v). A) Pore size; B) porosity (%); C) water content (24 h); D) repeated swelling profiles of pHEMA hydrogels: the gels were dried and swollen on succesive days and maintained their integrity. Statistical differences (* $P \leq 0.05$, ** $P \leq 0.01$, *** $P \leq 0.001$, **** $P \leq 0.0001$) are indicated

Table 2. Contact angles of the pHEMA hydrogels having different water contents in reaction mixture

Water content in reaction mixture (%)	Contact angles (°)
44	50.8 ± 15.4
50	31.0 ± 7.6
55	17.8 ± 10.2
58	6.2 ± 4.5

Mechanical properties of pHEMA hydrogels

Mechanical properties of the pHEMA are presented in Table 3. Tensile modulus of the hydrogels prepared with different water contents were seen to decrease as the water content of the preparation medium increased (from 548.6 kPa ± 23.4 kPa to 383.2 kPa ± 18.9 kPa). In addition, UTS of the pHEMA cylinders were also decreased to its half when the water content in the preparation medium was more than 50%.

Table 3. Mechanical properties of pHEMA hydrogels prepared with different water contents in reaction mixture

Water content in reaction mixture (%)	Tensile modulus (kPa)	Ultimate tensile strength (kPa)
44	548.6 ± 23.4	442.1 ± 75.1
50	570.9 ± 92.1	501.8 ± 93.7
55	431.4 ± 7.5	289.1 ± 13.7
58	383.2 ± 18.9	283.1 ± 35.1

In vitro studies

SC proliferation on pHEMA hydrogels

SC attachment and viability on pHEMA with 50% water content were studied with MTT cytotoxicity assay and live-dead analysis. The cell numbers were determined 24 h after cell seeding (5×10^4) (Figure 8). On pHEMA hydrogels, about 70% of the planted cells were discovered to be adhered. After 7 days, there were 5 times as many cells on the pHEMA as there were in the attached sample. The number almost doubled during the course of the following 7 days, and in the last week, it climbed slightly less. All of the cell number increases were determined to be statistically significant. Results of a 3-week live-dead assay using SCs on pHEMA hydrogels are shown in Figure 9A. On day 7, a significant portion of the seeded cells were able to adhere to and grow on the hydrogels (Figure 9A–F). They were dispersed over the pHEMA coated with collagen on day 14 (Figure 9G–I). The living cell fraction of the SCs is growing over time, as seen in Figure 9B. It demonstrates that SCs can adhere to and proliferate on pHEMA.

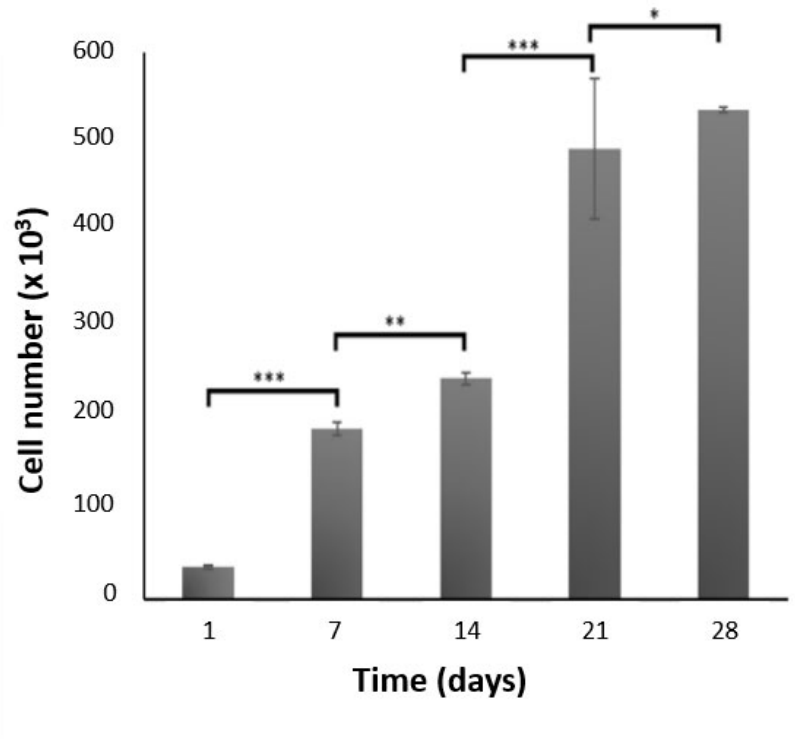

Figure 8. Proliferation of SCs on pHEMA hydrogels (MTT test). Statistical differences (* $P \leq 0.05$, ** $P \leq 0.01$, *** $P \leq 0.001$) are indicated

Proliferation of SH-SY5Y neuroblastoma cells in GelMA-HaMA IPNs

SH-SY5Y cells were chosen as a substitute for neural cell to study their behavior in the nerve conduit prepared. Film versions of GelMA-HaMA gels were developed for experiments on cell adhesion and proliferation. Almost 70% of the cells had adhered by the first day. The cells were able to grow exponentially on IPN surfaces as seen by the weekly cell number doubling or tripling (Figure 10). A two-week live-dead cell viability assay (Figure 11A) was carried out, and ImageJ was used to count the number of cells visible on the micrographs. Indicating that the hydrogel for the cells was cytocompatible, the live cell percentage of the cells was above 80% for the first week and above 90% on the second and third weeks (Figure 11B).

In vitro cell staining on the final conduit

Cells were stained to study cell proliferation and cell-material and cell-cell interactions. In order to obtain final cell including structure SH-SY5Y cell containing IPN was prepared and placed into the proximal end of

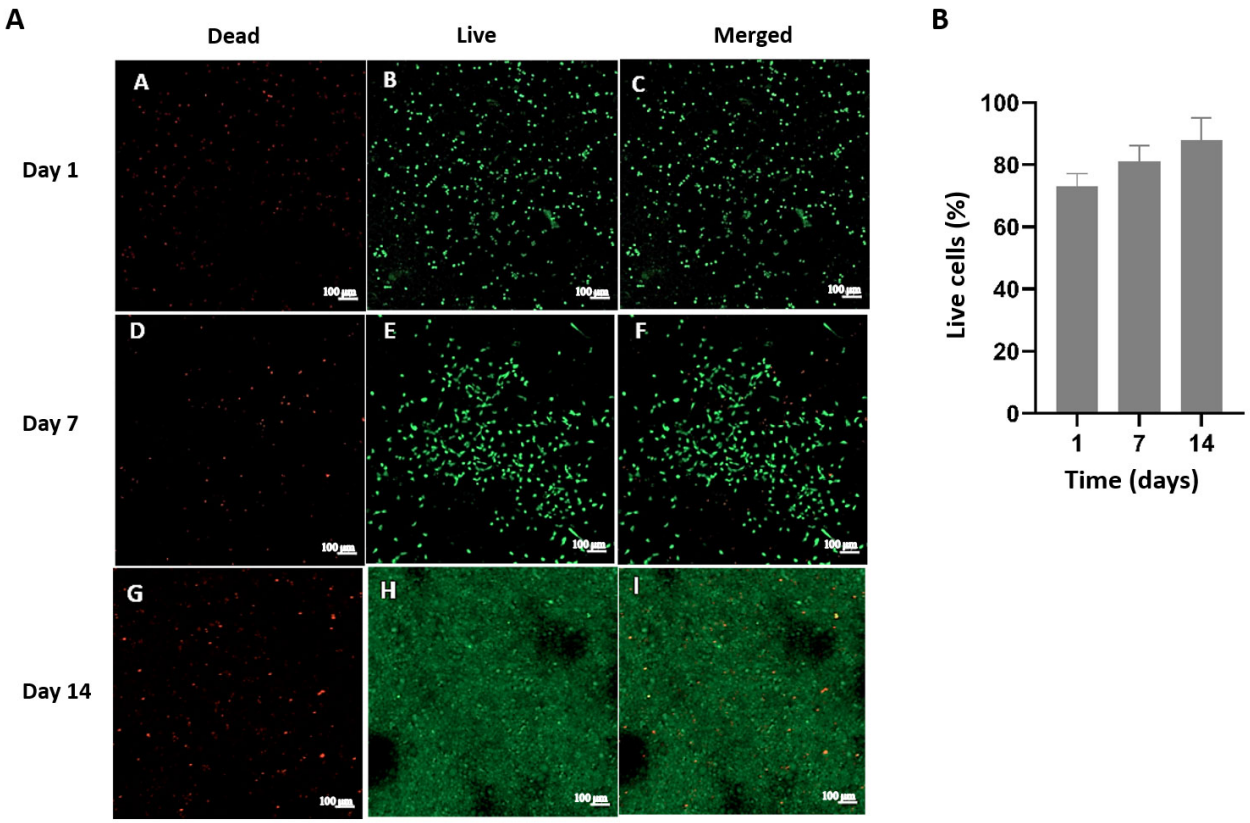

Figure 9. Live-dead analysis of SCs on pHEMA. Confocal micrographs of A) Dead and live cells and merged form of SCs (2 weeks). Scale bar: 100 µm; B) quantitative analysis of SCs on pHEMA hydrogels by using ImageJ software

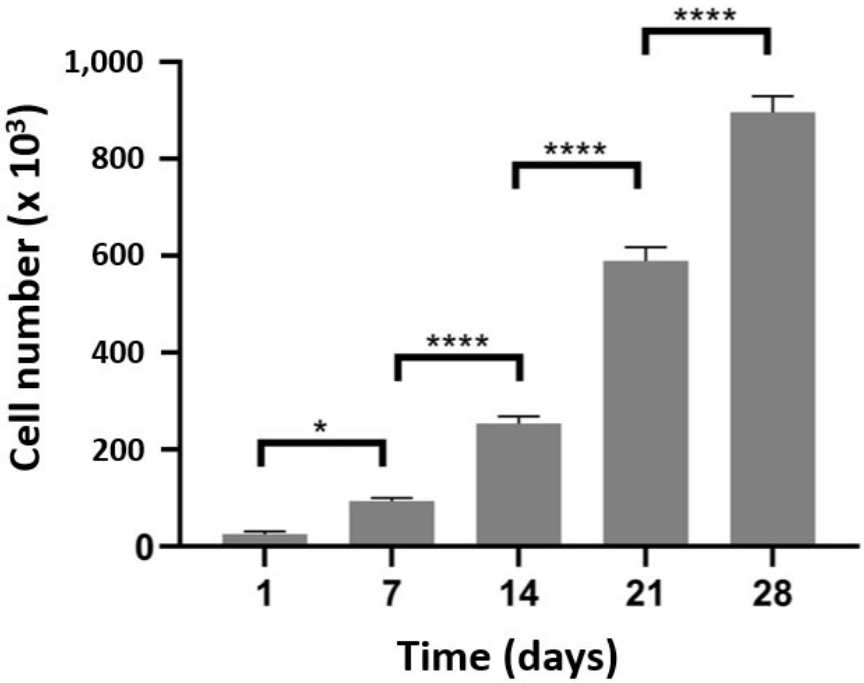

Figure 10. Proliferation of SH-SY5Ycells in GelMA-HaMA IPNs (MTT test) for 4 weeks. Statistical differences (* $P \leq 0.05$, ** $P \leq 0.01$, *** $P \leq 0.001$) are indicated

the pHEMA cylinder. The central and distal parts of the pHEMA tubes were filled with cell free IPNs. For the actin cytoskeleton the cells were stained with FITC-phalloidin and with DAPI for nucleus. The cells were examined for 3 weeks to study the ability of migration through the conduit (Figure 12). At the end of 7 days of incubation after placing cell containing IPNs in pHEMA tubes, cells had started to migrate through the conduit towards the distal end. On day 14 it was possible to see the cells throughout the cylinder. At the end of day 21 number of the cells at the distal part had increased (Figure 12).

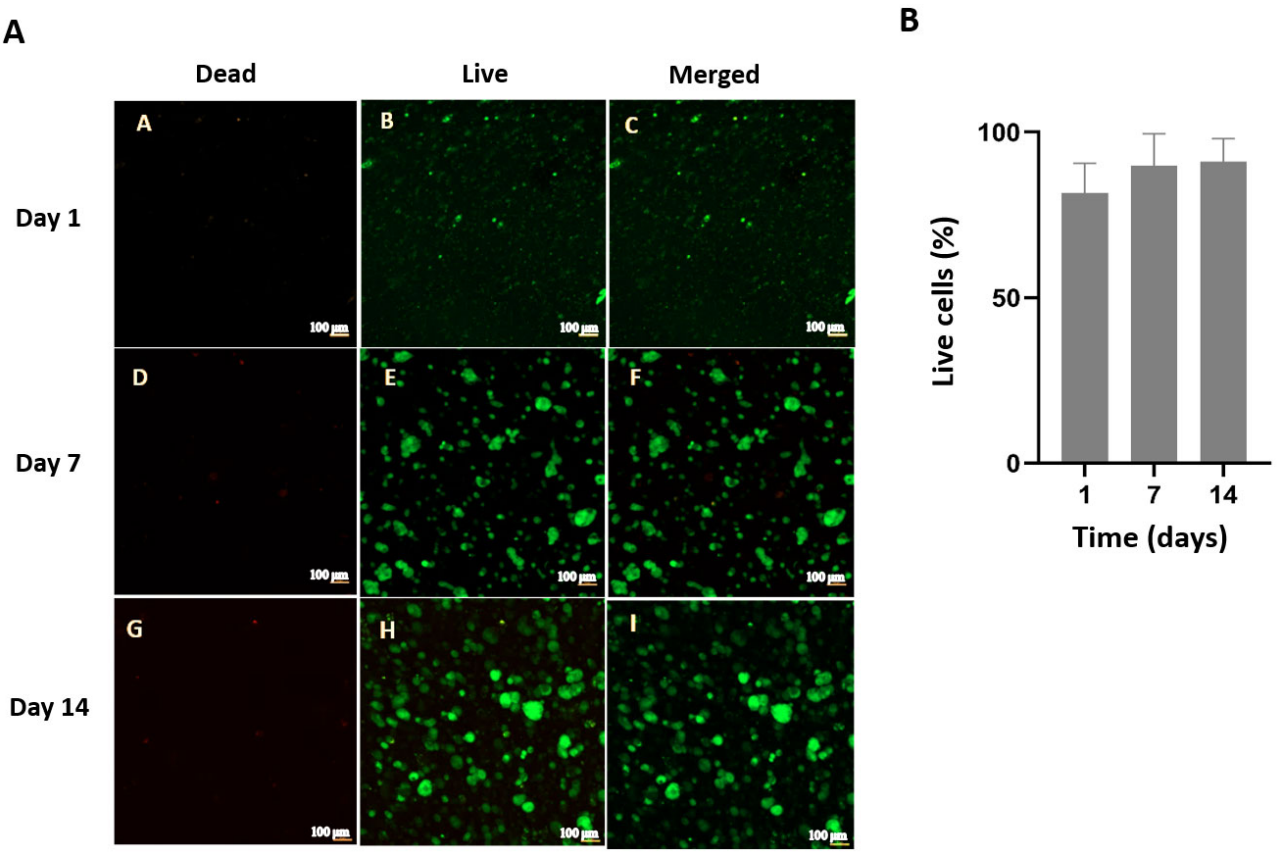

Figure 11. Live-dead analysis of SH-SY5Y cells in GelMA-HaMA IPNs. Confocal micrographs of A) Dead and live cells and merged form of SH-SY5Y cells (2 weeks). Scale bar: 100 µm; B) quantitative analysis of SH-SY5Y cells in GelMA-HaMA IPNs by using ImageJ software

β-III Tubulin and NeuN antibody staining

The present study SH-SY5Y cells were stained with both early (β-III tubulin) and late (NeuN) neuronal markers to evaluate their cellular state (Figure 13). NeuN expression was increased in 14 days of incubation, because it is a late neuronal marker. However, no significant increase was observed between days 7 and 14 in terms of β-tubulin.

Netrin-1 effect on SH-SY5Y cells

In the GelMA-HaMA IPNs, the SH-SY5Y cells were able to migrate through the pHEMA conduit and form neurite extensions in the current study. The neurite extensions, however, were not directed (Figure 12). The protein netrin-1 was loaded to the distal end of the conduit in order to direct the extensions. On days 7 and 14 following netrin-1 loading, the neurite extension was examined using β-III tubulin antibody staining. With better aligned extensions through the nerve conduit, SH-SY5Y cells began to stretch their extensions toward the distal end (Figure 14, yellow arrows).

Discussion

Peripheral nerve injury, caused by physical trauma can result in loss of neural communication. As a result of any acute nerve injury, neuronal capabilities may be lost. The nerve can regenerate its own damaged axons through complicated mechanisms including Wallerian regeneration [2]. In the absence of segmentation loss or when the gap is significantly smaller than 3 mm, regeneration and repair in the PNS begin quite rapidly in the presence of moderate damage. In more severe injuries, there is an initial shock phase, followed by months of regeneration and repair ending with unsuccessful regeneration due to axonal sprouting. SCs are essential for promoting regeneration as they produce more cell surface adhesion molecules and form basement membranes containing ECM proteins [3]. Another option for lesions less than 3 mm is end-to-end suturing. However, suturing method can create tension that lead to in loss of neuronal communication in

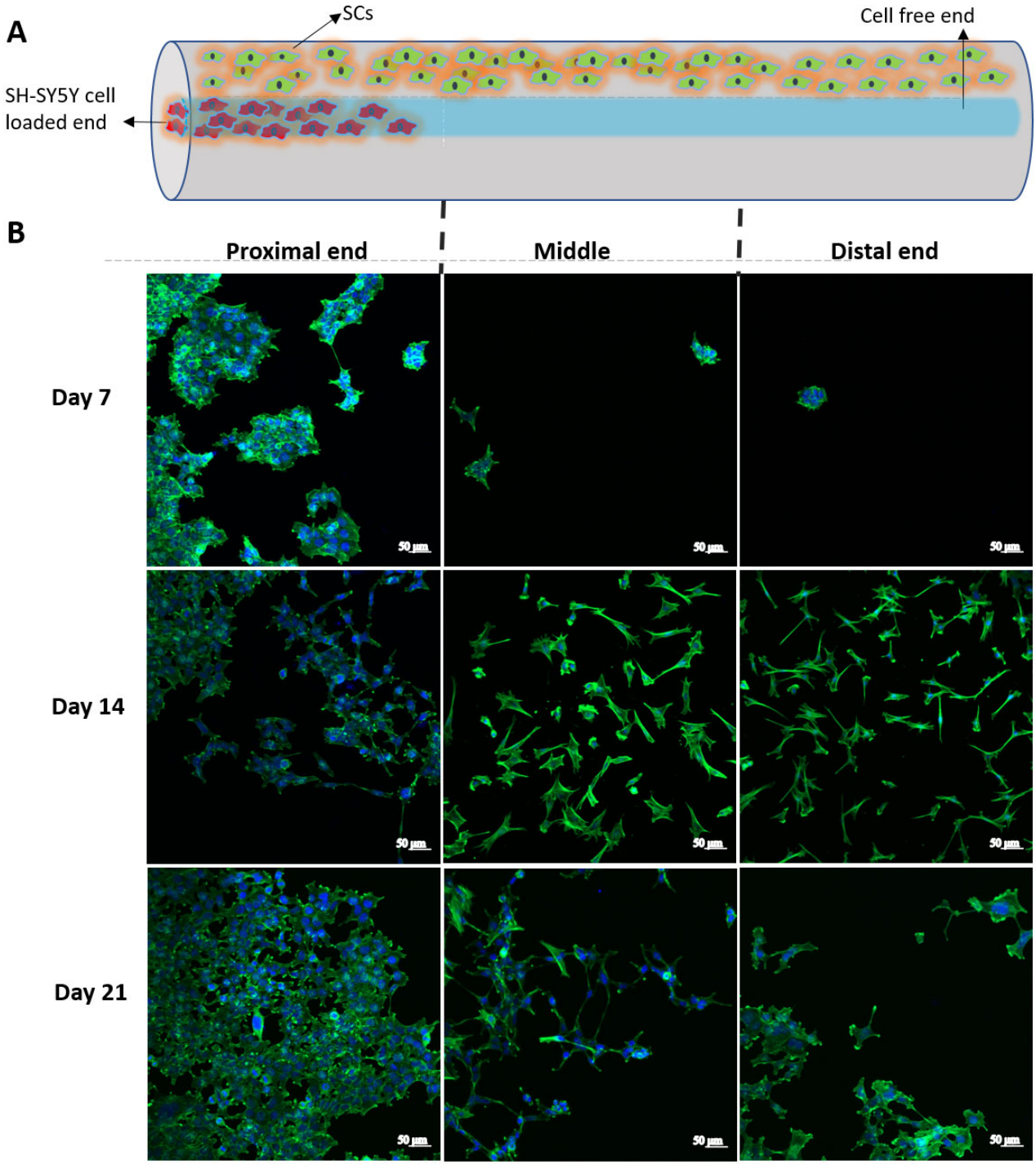

Figure 12. Distribution of SH-SY5Y cells in the IPN in the neve guide. A) Schematic representation of a conduit and the cellss; B) SH-SY5Y cell proliferation in proximal, middle and distal parts of the conduit structure on days 7, 14 and 21. Scale bar: 50 µm

larger gaps. When end-to-end suturing is not possible, grafting methods are used. On the other hand, grafting materials (autografts, allografts, xenografts) have some drawbacks like cross-contamination, donor site morbidity, immune rejection and limited supply of donors. To overcome these limitations, researchers have focused on the construction of nerve conduits for axonal regeneration after nerve injury [5, 7]. These conduits are fabricated using synthetic or natural polymers. In some cases hybrid constructions are considered to adapt the mechanical and structural properties for nerve regeneration [13].

In the present study, a cylindrical nerve guidance conduit with an inner IPN structure is presented. The outer tube was made of pHEMA coated with collagen for cell attachment and the inner IPN was made by combining of GelMA and HaMA. As supportive materials, SCs and netrin-1, a molecule involved in axon guidance and cell migration, were used. *In situ* and *in vitro* characterization of the outer pHEMA and inner

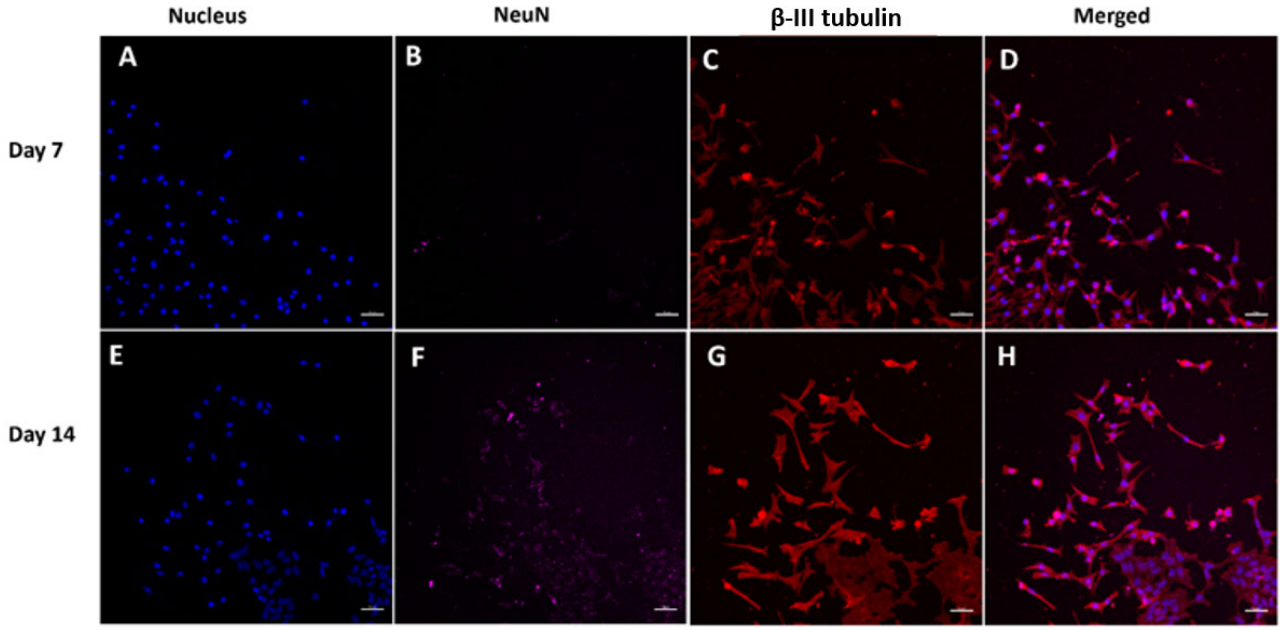

Figure 13. Increase in neuronal markers (NeuN and β-III tubulin) in SH-SY5Y cells in the nerve conduits. (A–D) Day 7; (F–H) day 14. The images were taken from the proximal end of the conduits. Scale bar: 50 μm

GelMA-HaMA IPN structures was performed to determine their suitability for axonal regeneration after nerve injury in terms of degradation, water content, mechanical properties, hydrophilicity and porosity.

GelMA-HaMA IPN structures were prepared using different combinations of GelMA and HaMA. The water contents of all IPNs were very similar to each other; they were above 80%, which is suitable for soft tissue applications such as neural differentiation and neurite outgrowth [42–44]. It was also previously shown that GelMA based hydrogels had ability to swell up to 100 times over their lyophilized dried weights. Compared to the pure GelMA and HaMA hydrogels, the swelling ability of IPN structure was increased by combining GelMA and HaMA. The IPN with the composition of GelMA-HaMA in the ratio of 90:10 showed a percentage swelling about 900%. The degradation profiles of the IPNs were examined in both PBS and cell culture media. Increasing the fraction of HaMA in IPN structure increased the weight loss rate. This can be explained by the crosslinking efficiencies of GelMA and HaMA. The methacryloyl groups introduced to GelMA and HaMA are important for the crosslinking density. Degrees of methacrylation are 94% ± 2% and 60% ± 7%, for GelMA and HaMA, respectively. Thus, increasing the HaMA fraction in the IPN results in a decrease in the amount of MA groups in IPNs, and therefore, in the crosslinking efficiency, resulting in a higher rate of degradation. During degradation and cell ingrowth, cells deposit new ECM that supports tissue regeneration. Therefore, timing for degradation is also important; degradation time should coincide with the time of ECM deposition and cell proliferation [45]. Slow degradation may hinder ECM deposition, while too rapid degradation may result in a mechanically unstable structure due to the lack of ECM molecules. The present results showed that the IPN with GelMA-HaMA in a ratio of 85:15 had a water content of 80% and a swelling capacity of 800% and degraded within 4 weeks, which was suitable for the refeneration of neural tissue; the degradation of the IPN structure as a sacrificial material should aloe the expansion of rebenerating axons. Therefore, it was selected for the construction of final conduit. Similar degradation results were observed in a different study in which the sacrificial material GelMA was used to develop a scaffold; this material was thought to be suitable for cell ingrowth during axon regeneration [37, 46–48]. The outer pHEMA tube was optimized for porosity, water content, mechanical strength and hydrophilicity. Hydration and mechanical support are provided by the hydrogels in swollen state. In addition to mimic natural tissues, it is possible to tune their swelling and stiffness. For cell ingrowth, nutrient diffusion and vascularization, interconnected porous structures are the most suitable environment. Scaffold porosities, pore size distributions, and average pore dimensions are crucial [49–52]. The preparation mixture's water content changed to find the best conduit for neuronal regrowth. For water contents of 44%, 50%, 55%, and 58%, respectively, the hydrogels' porosities were determined to be 17%,

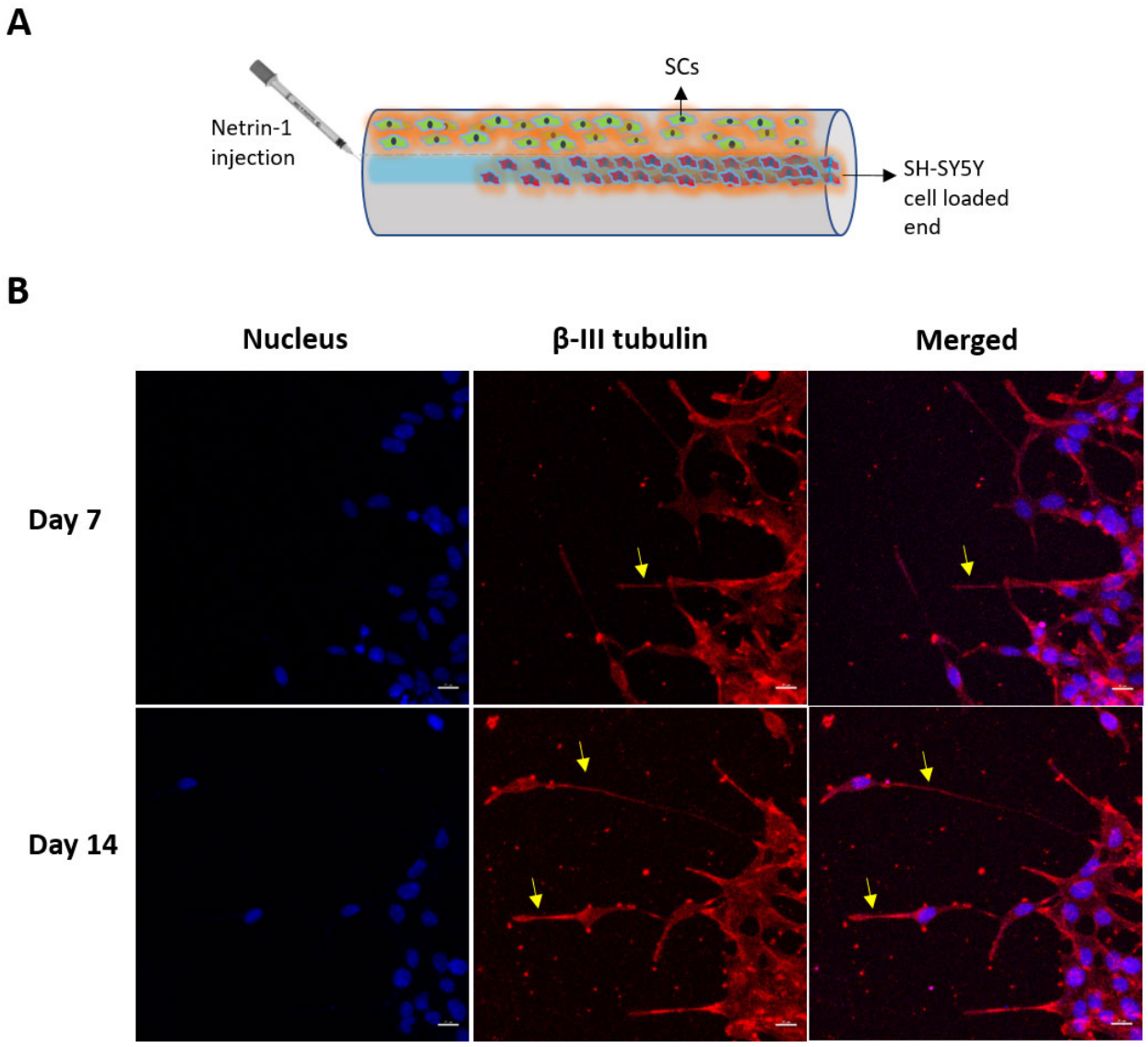

Figure 14. β-III Tubulin expression of SH-SY5Y cells. A) Schematic representation of a conduit showing cell seeding and netrin-1 loading sites; B) SH-SY5Y cells in the nerve conduits presenting nucleus (DAPI, blue), β-III tubulin (β-III tubulin antibody, red) and merged images. Yellow arrows show extensions. The images were taken from the proximal end of the conduits. Scale bar: 20 μm

33%, 52%, and 50%, and their pore diameters to be 40.75 μm ± 8.59 μm, 55.09 μm ± 7.15 μm, 15.24 μm ± 3.05 μm and 15.44 μm ± 2.05 μm. Thus, the porous structure of pHEMA conduit in the present case is especially useful for nutrient permeation, waste removal and for ECM protein deposition. SCs seeded on the pHEMA conduit are expected to produce growth factors for axonal regeneration and elongation and thus the growth factors produced go through the walls of the conduit through the pores interconnected with each other along the length of the tubular conduit [53]. In order to produce nerve guides, hydrogels with an interconnected porosity structure and a water content of 50% were selected.

It was observed that the equilibrium water content of pHEMA tubes with different water contents of the preparation mixture increased up to 52% with increasing water content of the preparation mixture. Since solute diffusion and mechanical properties of scaffolds are affected by variations in equilibrium water content, 52% was considered appropriate for nerve conduit applications [54]. The pHEMA tubes fabricated in this study are capable of repeated swelling without producing hysteresis, indicating that they maintain their integrity. This makes the tubes a good choice for soft tissue engineering applications [18]. Protein adsorption and cell adhesion are directly related to the hydrophilicity of a scaffold material. Therefore, for cell attachment and growth, the contact angle is an important parameter [16]. Cells are mostly able to adhere to highly hydrophilic surfaces, but the cell-cell interaction is unfavorable due to the good interaction

between the cells and the surface. Moreover, mostly hydrophobic surfaces are not preferable for biomedical applications because cells cannot attach to these surfaces [55]. In the present study, the contact angles of the surfaces were shown to be suitable for SC attachment (31.0° ± 7.6° for the pHEMA prepared with 50% water).

Another important parameter for the use of biomaterials as medical devices is suitable mechanical properties, with tensile strength mainly influencing the suturing of hydrogel implants during surgery [44]. In the literature, acellular nerve tissue is reported to have a tensile strength of 1,400 kPa and a tensile modulus of 576 kPa [19]. Acellular tissue has a much lower UTS than the conduits in the current study, while pHEMA prepared with 44% and 50% water content had tensile modulus values equivalent to those of nerve tissue (548.6 kPa ± 23.4 kPa and 570.9 kPa ± 92.1 kPa, respectively). Thus, the pHEMA tubes in the study are suitable for cell migration and attachment, as well as for suturing in future operations for nerve injury as a substitute material for the application of nerve tissue.

SCs were seeded on in a pHEMA tube coated with collagen to facilitate axonal regrowth. Nearly 70% of the cells were able to attach to surfaces and proliferate. SH-SY5Y cells were used as a model for axonal regeneration and seeded into GelMA-HaMA IPN constructs. It was found that the majority of SH-SY5Y cells were also able to attach and proliferate. Cell cytoskeleton and nucleus were stained and examined under CSLM to study cell proliferation and migration after construction of the final conduit (Figure 1). After 3 weeks, the cells were shown to be able to migrate to the mid and distal ends. In addition, the appearance of neurite outgrowth and cell-to-cell communication was considered a positive development, suggesting that the conduit construction containing GelMA-HaMA IPN may be able to accommodate expanding neurons for axonal regeneration in case of injury. In addition, SH-SY5Y cells were examined using neuronal marker labeling. Early neuronal markers include β-III tubulin, a microtubule element, while late neuronal markers include NeuN, a neuron-specific nuclear protein [56, 57]. NeuN expression of SH-SY5Y cells in our study showed increase in 2 weeks. Quantitative immunofluorescence quantification in ImageJ was performed through dividing integrated density of the fluorescence coming from NeuN expression by total cell number following thresholding [58]. It was seen that the intensity was increased 20-fold (from 0.1% to 2%). Actin and microtubule dynamics are involved in the formation of the growth cone during neurite outgrowth. The expansion of developing neurites was seen using β-III tubulin antibody labeling. Hyaluronan and carbon nanotubes were used in Ruiz et al. [59] nerve conduit, and the suitability of the structures for regenerating tubular neural structures was evaluated. They concluded that the nerves on the neural tubes were capable of producing β-tubulin and that the presence of neuronal markers made the neural tubes suitable for use in nerve regeneration. In the present study, the expression of β-tubulin was observed at both day 7 and day 14. The fluorescence intensities of the images did not show any significant difference (23% and 26%, respectively) showing that SH-SY5Y cells were able to produce neurites. Other studies have demonstrated the efficiency of conduits in relation to neurite formation using the anti-β-III tubulin marker, and they all concluded that higher β-tubulin production is favorable for nerve conduits used for axon regeneration after peripheral injury [60–64]. In addition to SCs, the netrin-1 protein was also injected into the distal part of the pHEMA tube as a supporting molecule. In vertebrates, circumferential axonal projections can be directed by netrin proteins [28]. Netrin-1, originally discovered as a traditional axonal guidance protein, is critical for controlling axon pathfinding and migration in neurons. In the present study, on day 7, the extensions were found to extend up to 150 μm, while on day 14 they reached 350–400 μm. In a study by Cai et al. [65], a concentration gradient of netrin-1 was generated by submerging the lower part of a nerve conduit using a controlled diffusion method. The results showed that biological gradients can significantly enhance axon regeneration by triggering axon attraction through intracellular signaling responses and promoting axon extension. In addition, Huang et al. [28] developed a conductive double network (DN) hydrogel scaffold supported by a graphene mesh and enriched in netrin-1. GelMA and alginate were intertwined to produce the hydrogel, which serves as a reservoir for netrin-1. They concluded that netrin-1 loading was even more effective than autologous grafts in improving peripheral nerve regeneration and denervated muscle repair. The results of the present study showed that at the end of the second week, the outgrowths of SH-SY5Y cells were concentrated at the distal end where the netrin-1 protein had been

injected. In conclusion, the presented pHEMA tube with GelMA-HaMA-IPN structure is a promising nerve guidance tube considering the properties such as mechanical strength, swelling capacity, degradation profile, and hydrophilicity. SCs seeded on the pHEMA tube along with the IPN structure supported the migration of SH-SY5Y cells, model cells for axonal regeneration. In addition, injection of netrin-1 at the distal end of the tube directed the neural projections of SH-SY5Y cells toward the end. Future studies will test the completed conduit *in vivo*. It is expected to be useful for peripheral nerve regeneration.

Abbreviations

^{1}H-NMR: ^{1}H-nuclear magnetic resonance

BSA: bovine serum albumin

DAPI: 4',6-diamidino-2-phenylindole dihydrochloride

DM: degree of methacrylation

DMEM: Dulbecco's Modified Eagles Medium

ECM: extracellular matrix

FBS: fetal bovine serum

GelMA: methacrylated gelatin

HA: hyaluronic acid

HaMA: methacrylated hyaluronic acid

IPN: interpenetrating network

MA: methacrylic acid

MTT: 3-(4,5-dimethylthiazol-2-yl)-2,5-diphenyltetrazolium bromide

PBS: phosphate buffered saline

pHEMA: poly(2-hydroxyethylmethacrylate)

PNS: peripheral nervous system

RT: room temperature

SCs: Schwann cells

SEM: scanning electron microscope

UTS: ultimate tensile strength

UV: ultraviolet light

Declarations

Acknowledgments

We acknowledge the support by METU CoE in Biomaterials and Tissue Engineering (BIOMATEN) for the use of the facilities and materials. We also acknowledge Department of Bioengineering and Genetics, Gumushane University, Turkey for the opportunity to study at METU.

Author contributions

DAS: Resources, Data curation, Formal analysis, Investigation, Methodology, Validation, Writing—original draft. CDS: Validation, Writing—review & editing, Supervision. VH: Conceptualization, Methodology, Validation, Visualization, Writing—review & editing, Supervision. All authors read and approved the submitted version.

Conflicts of interest

The authors declare that they have no conflicts of interest.

Ethical approval

Not applicable.

Consent to participate

Not applicable.

Consent to publication

Not applicable.

Availability of data and materials

The raw data supporting the conclusions of this manuscript will be made available by the authors, without undue reservation, to any qualified researcher.

Funding

This work was supported by Strategy and Budget Department of Turkiye Republic [BAP-08-11-KB.2016K-121520]. The funders had no role in study design, data collection and analysis, decision to publish, or preparation of the manuscript.

References

1. Li NY, Onor GI, Lemme NJ, Gil JA. Epidemiology of peripheral nerve ınjuries in sports, exercise, and recreation in the United States, 2009 – 2018. Phys Sportsmed. 2021;49:355–62.
2. Lopes B, Sousa P, Alvites R, Branquinho M, Sousa AC, Mendonça C, et al. Peripheral nerve injury treatments and advances: one health perspective. Int J Mol Sci. 2022;23:918.
3. Baradaran A, El-Hawary H, Efanov JI, Xu L. Peripheral nerve healing: so near and yet so far. Semin Plast Surg. 2021;35:204–10.
4. Wieringa PA, Gonçalves de Pinho AR, Micera S, van Wezel RJA, Moroni L. Biomimetic architectures for peripheral nerve repair: a review of biofabrication strategies. Adv Healthc Mater. 2018;7:e1701164.
5. Krauss EM, Weber RV, Mackinnon SE. 52 - Nerve injury, repair, and reconstruction. In: Farhadieh RD, Bulstrode NW, Mehrara BJ, Cugno S, editors. Plastic surgery - principles and practice. Elsevier; 2022. pp. 803–25.
6. Kasper M, Deister C, Beck F, Schmidt CE. Bench-to-bedside lessons learned: commercialization of an acellular nerve graft. Adv Healthc Mater. 2020;9:e2000174.
7. Narayan SK, Arumugam M, Chittoria R. Outcome of human peripheral nerve repair interventions using conduits: a systematic review. J Neurol Sci. 2019;396:18–24.
8. Xu H, Yu Y, Zhang L, Zheng F, Yin Y, Gao Y, et al. Sustainable release of nerve growth factor for peripheral nerve regeneration using nerve conduits laden with bioconjugated hyaluronic acid-chitosan hydrogel. Composites, Part B. 2022;230:109509.
9. Wolfe EM, Mathis SA, Ovadia SA, Panthaki ZJ. Comparison of collagen and human amniotic membrane nerve wraps and conduits for peripheral nerve repair in preclinical models: a systematic review of the literature. J Reconstr Microsurg. 2023;39:245–53.
10. Xiang L, Cui W. Biomedical application of photo-crosslinked gelatin hydrogels. J Leather Sci Eng. 2021; 3:1–24.
11. Alvites RD, Branquinho MV, Sousa AC, Amorim I, Magalhães R, João F, et al. Combined use of chitosan and olfactory mucosa mesenchymal stem/stromal cells to promote peripheral nerve regeneration *in vivo*. Stem Cells Int. 2021;2021:6613029.

12. Abdelbasset WK, Jasim SA, Sharma SK, Margiana R, Bokov DO, Obaid MA, et al. Alginate-based hydrogels and tubes, as biological macromolecule-based platforms for peripheral nerve tissue engineering: a review. Ann Biomed Eng. 2022;50:628–53.
13. Li A, Pereira C, Hill EE, Vukcevich O, Wang A. *In vitro*, *in vivo* and *ex vivo* models for peripheral nerve ınjury and regeneration. Curr Neuropharmacol. 2022;20:344–61.
14. Roca FG, Santos LG, Roig MM, Medina LM, Martínez-Ramos C, Pradas MM. Novel tissue-engineered multimodular hyaluronic acid-polylactic acid conduits for the regeneration of sciatic nerve defect. Biomedicines. 2022;10:963.
15. Onode E, Uemura T, Hama S, Yokoi T, Okada M, Takamatsu K, et al. Nerve-end capping treatment with a polyglycolic acid conduit for rat sciatic neuroma: a preliminary report. J Reconstr Microsurg. 2022; 38:711–20.
16. Grijalvo S, Díaz DD. Graphene-based hybrid materials as promising scaffolds for peripheral nerve regeneration. Neurochem Int. 2021;147:105005.
17. Pozzobon LG, Sperling LE, Teixeira CE, Malysz T, Pranke P. Development of a conduit of PLGA-gelatin aligned nanofibers produced by electrospinning for peripheral nerve regeneration. Chem Biol Interact. 2021;348:109621.
18. Dursun Usal T, Yesiltepe M, Yucel D, Sara Y, Hasirci V. Fabrication of a 3D printed PCL nerve guide: *in vitro* and *in vivo* testing. Macromol Biosci. 2022;22:e2100389.
19. Borschel GH, Kia KF, Kuzon WM Jr, Dennis RG. Mechanical properties of acellular peripheral nerve. J Surg Res. 2003;114:133–9.
20. Ma X, Wang M, Ran Y, Wu Y, Wang J, Gao F, et al. Design and fabrication of polymeric hydrogel carrier for nerve repair. Polymers (Basel). 2022;14:1549.
21. Zare M, Bigham A, Zare M, Luo H, Rezvani Ghomi E, Ramakrishna S. pHEMA: an overview for biomedical applications. Int J Mol Sci. 2021;22:6376.
22. Velasco-Rodriguez B, Diaz-Vidal T, Rosales-Rivera LC, García-González CA, Alvarez-Lorenzo C, Al-Modlej A, et al. Hybrid methacrylated gelatin and hyaluronic acid hydrogel scaffolds. Preparation and systematic characterization for prospective tissue engineering applications. Int J Mol Sci. 2021;22: 6758.
23. Dodla MC, Alvarado-Velez M, Mukhatyar VJ, Bellamkonda RV. Peripheral nerve regeneration. Chapter 69 - Peripheral nerve regeneration. In: Atala A, Lanza R, Mikos AG, Nerem R, editors. Principles of regenerative medicine (third edition). Boston: Academic Press; 2019. pp. 1223–36.
24. Min Q, Parkinson DB, Dun XP. Migrating Schwann cells direct axon regeneration within the peripheral nerve bridge. Glia. 2021;69:235–54.
25. Wu P, Tong Z, Luo L, Zhao Y, Chen F, Li Y, et al. Comprehensive strategy of conduit guidance combined with VEGF producing Schwann cells accelerates peripheral nerve repair. Bioact Mater. 2021;6: 3515–27.
26. Endo T, Kadoya K, Suzuki T, Suzuki Y, Terkawi MA, Kawamura D, et al. Mature but not developing Schwann cells promote axon regeneration after peripheral nerve injury. NPJ Regen Med. 2022;7:12.
27. Jessen KR, Mirsky R. Schwann cells in nerve repair and regeneration. In: Phillips JB, Hercher D, Hausner T, editors. Peripheral nerve tissue engineering and regeneration. Springer, Cham; 2022. pp. 385–401.
28. Huang Q, Cai Y, Zhang X, Liu J, Liu Z, Li B, et al. Aligned graphene mesh-supported double network natural hydrogel conduit loaded with netrin-1 for peripheral nerve regeneration. ACS Appl Mater Interfaces. 2021;13:112–22.
29. Xie HR, Hu LS, Li GY. SH-SY5Y human neuroblastoma cell line: *in vitro* cell model of dopaminergic neurons in Parkinson's disease. Chin Med J (Engl). 2010;123:1086–92.

30. Cerda-Sumbarda YD, Zapata-Gonzalez I, Licea-Claverie A, Zizumbo-Lopez A, F. Ramos-de Valle L, Espinoza-Martínez A. Poly(hexylacrylate)$_{Core}$-poly(ethyleneglycol methacrylate)$_{Shell}$ nanogels as fillers for poly(2-hydroxyethyl methacrylate) nanocomposite hydrogels. Polym Eng Sci. 2019;59:170–81.
31. Shirahama H, Lee BH, Tan LP, Cho NJ. Precise tuning of facile one-pot gelatin methacryloyl (GelMA) synthesis. Sci Rep. 2016;6:31036.
32. Smeds KA. Synthesis, characterization, and biomedical applications of novel photocrosslinkable hydrogels and biodendrimers [dissertation]. Duke University; 2002.
33. Twarużek M, Zastempowska E, Soszczyńska E, Ałtyn I. The use of *in vitro* assays for the assessment of cytotoxicity on the example of MTT test. Folia Biol. 2018;14:23–32.
34. Hoch E, Schuh C, Hirth T, Tovar GE, Borchers K. Stiff gelatin hydrogels can be photo-chemically synthesized from low viscous gelatin solutions using molecularly functionalized gelatin with a high degree of methacrylation. J Mater Sci Mater Med. 2012;23:2607–17.
35. Shie MY, Lee JJ, Ho CC, Yen SY, Ng HY, Chen YW. Effects of gelatin methacrylate bio-ink concentration on mechano-physical properties and human dermal fibroblast behavior. Polymers (Basel). 2020;12: 1930.
36. Yousefi F, Kandel S, Pleshko N. Infrared spectroscopic quantification of methacrylation of hyaluronic acid: a scaffold for tissue engineering applications. Appl Spectrosc. 2018;72:1455–66.
37. Dursun Usal T, Yucel D, Hasirci V. A novel GelMA-pHEMA hydrogel nerve guide for the treatment of peripheral nerve damages. Int J Biol Macromol. 2019;121:699–706.
38. Tutar R, Yüce-Erarslan E, İzbudak B, Bal-Öztürk A. Photocurable silk fibroin-based tissue sealants with enhanced adhesive properties for the treatment of corneal perforations. J Mater Chem B. 2022;10: 2912–25.
39. Zamboni F, Okoroafor C, Ryan MP, Pembroke JT, Strozyk M, Culebras M, et al. On the bacteriostatic activity of hyaluronic acid composite films. Carbohydr Polym. 2021;260:117803.
40. Khurana B, Ouk TS, Lucas R, Senge MO, Sol V. Photosensitizer-hyaluronic acid complexes for antimicrobial photodynamic therapy (aPDT). J Porphyr Phthalocyanines. 2022;26:585–93.
41. Correa S, Grosskopf AK, Lopez Hernandez H, Chan D, Yu AC, Stapleton LM, et al. Translational applications of hydrogels. Chem Rev. 2021;121:11385–457.
42. O'Grady BJ, Balotin KM, Bosworth AM, McClatchey PM, Weinstein RM, Gupta M, et al. Development of an N-cadherin biofunctionalized hydrogel to support the formation of synaptically connected neural networks. ACS Biomater Sci Eng. 2020;6:5811–22.
43. Xiao S, Zhao T, Wang J, Wang C, Du J, Ying L, et al. Gelatin methacrylate (GelMA)-based hydrogels for cell transplantation: an effective strategy for tissue engineering. Stem Cell Rev Rep. 2019;15:664–79.
44. Noh I, Kim N, Tran HN, Lee J, Lee C. 3D printable hyaluronic acid-based hydrogel for its potential application as a bioink in tissue engineering. Biomater Res. 2019;23:3.
45. Roth JG, Huang MS, Li TL, Feig VR, Jiang Y, Cui B, et al. Advancing models of neural development with biomaterials. Nat Rev Neurosci. 2021;22:593–615.
46. Camci-Unal G, Cuttica D, Annabi N, Demarchi D, Khademhosseini A. Synthesis and characterization of hybrid hyaluronic acid-gelatin hydrogels. Biomacromolecules. 2013;14:1085–92.
47. Wang Y, Ma M, Wang J, Zhang W, Lu W, Gao Y, et al. Development of a photo-crosslinking, biodegradable GelMA/PEGDA hydrogel for guided bone regeneration materials. Materials (Basel). 2018;11:1345.
48. Wang Y, Lin C. Study on properties of 3D-printed GelMA hydrogel scaffolds with different nHA contents. J Bioact Compat Polym. 2022;37:392–405.
49. Elkhoury K, Morsink M, Sanchez-Gonzalez L, Kahn C, Tamayol A, Arab-Tehrany E. Biofabrication of natural hydrogels for cardiac, neural, and bone tissue engineering applications. Bioact Mater. 2021;6: 3904–23.

50. Pooshidani Y, Zoghi N, Rajabi M, Haghbin Nazarpak M, Hassannejad Z. Fabrication and evaluation of porous and conductive nanofibrous scaffolds for nerve tissue engineering. J Mater Sci Mater Med. 2021;32:46.
51. Hasirci N, Kilic C, Kömez A, Bahcecioglu G, Hasirci V. Chapter 1: Hydrogels in regenerative medicine. In: Gels handbook. 2016. pp. 1–52.
52. Chen Y, Long X, Lin W, Du B, Yin H, Lan W, et al. Bioactive 3D porous cobalt-doped alginate/ waterborne polyurethane scaffolds with a coral reef-like rough surface for nerve tissue engineering application. J Mater Chem B. 2021;9:322–35.
53. Manoukian OS, Arul MR, Rudraiah S, Kalajzic I, Kumbar SG. Aligned microchannel polymer-nanotube composites for peripheral nerve regeneration: small molecule drug delivery. J Control Release. 2019; 296:54–67.
54. Kilic Bektas C, Hasirci V. Cell loaded GelMA:HEMA IPN hydrogels for corneal stroma engineering. J Mater Sci Mater Med. 2019;31:2.
55. Ferreira CL, Valente CA, Zanini ML, Sgarioni B, Ferreira Tondo PH, Chagastelles PC, et al. Biocompatible PCL/PLGA/Polypyrrole composites for regenerating nerves. Macromol Symp. 2019; 383:1800028.
56. Fath MK, Zahedi F, Hashemi ZS, Khalili S. Evaluation of differentiation quality of several differentiation inducers of bone marrow-derived mesenchymal stem cells to nerve cells by assessing expression of beta-tubulin 3 marker: a systematic review. Curr Stem Cell Res Ther. 2021;16:994–1004.
57. Luijerink L, Waters KA, Machaalani R. Immunostaining for NeuN does not show all mature and healthy neurons in the human and pig brain: focus on the hippocampus. Appl Immunohistochem Mol Morphol. 2021;29:e46–56.
58. Tenbaum S, Palmer HG, Arqués O, Chicote I, Puig I. Standardized relative quantification of ımmunofluorescence tissue staining. Research Square [Preprint]. 2012 [cited 2021 Nov 11]. Available from: https://doi.org/10.1038/protex.2012.008
59. Ruiz IM, Vilariño-Feltrer G, Mnatsakanyan H, Vallés-Lluch A, Monleón Pradas M. Development and evaluation of hyaluronan nanocomposite conduits for neural tissue regeneration. J Biomater Sci Polym Ed. 2021;32:2227–45.
60. Dong X, Liu S, Yang Y, Gao S, Li W, Cao J, et al. Aligned microfiber-induced macrophage polarization to guide schwann-cell-enabled peripheral nerve regeneration. Biomaterials. 2021;272:120767.
61. Ma Y, Wei C, Qi X, Pu Y, Dong L, Xu L, et al. *Schistosoma japonicum*-derived peptide SJMHE1 promotes peripheral nerve repair through a macrophage-dependent mechanism. Am J Transl Res. 2021;13: 1290–306.
62. Ramesh PA, Dhandapani R, Bagewadi S, Zennifer A, Radhakrishnan J, Sethuraman S, et al. Reverse engineering of an anatomically equivalent nerve conduit. J Tissue Eng Regen Med. 2021;15:998–1011.
63. Yang X, Huang L, Yi X, Huang S, Duan B, Yu A. Multifunctional chitin-based hollow nerve conduit for peripheral nerve regeneration and neuroma inhibition. Carbohydr Polym. 2022;289:119443.
64. Zhang H, Guo J, Wang Y, Shang L, Chai R, Zhao Y. Natural polymer-derived bioscaffolds for peripheral nerve regeneration. Advanced Functional Materials. 2022;32:2203829.
65. Cai Y, Huang Q, Wang P, Ye K, Zhao Z, Chen H, et al. Conductive hydrogel conduits with growth factor gradients for peripheral nerve repair in diabetics with non-suture tape. Adv Healthc Mater. 2022;11: e2200755.